Eur. Phys. J. C 28, 27–44 (2003)
Digital Object Identifier (DOI) 10.1140/epjc/s2002-01113-3

THE EUROPEAN PHYSICAL JOURNAL C

Higgs physics with a $\gamma\gamma$ collider based on CLIC 1

D. Asner[1], H. Burkhardt[2], A. De Roeck[2], J. Ellis[2], J. Gronberg[1], S. Heinemeyer[3], M. Schmitt[4], D. Schulte[2], M. Velasco[4], F. Zimmermann[2]

[1] Lawrence Livermore National Laboratory, Livermore, California 94550, USA
[2] CERN, 1211 Geneva 23, Switzerland
[3] Brookhaven National Laboratory, Upton, New York, USA
[4] Northwestern University, Evanston, Illinois 60201, USA

Received: 20 November 2001 /
Published online: 24 March 2003 –

Abstract. We present the machine parameters and physics capabilities of the CLIC Higgs Experiment (CLICHE), a low-energy $\gamma\gamma$ collider based on CLIC 1, the demonstration project for the higher-energy two-beam accelerator CLIC. CLICHE is conceived as a factory capable of producing around 20,000 light Higgs bosons per year. We discuss the requirements for the CLIC 1 beams and a laser backscattering system capable of producing a $\gamma\gamma$ total (peak) luminosity of 2.0 $(0.36) \times 10^{34}$ cm^{-2}s^{-1} with $E_{CM}(\gamma\gamma) \sim 115$ GeV. We show how CLICHE could be used to measure accurately the mass, $\bar{b}b$, WW and $\gamma\gamma$ decays of a light Higgs boson. We illustrate how these measurements may distinguish between the Standard Model Higgs boson and those in supersymmetric and more general two-Higgs-doublet models, complementing the measurements to be made with other accelerators. We also comment on other prospects in $\gamma\gamma$ and $e^-\gamma$ physics with CLICHE.

1 Introduction

CLIC [1] is a project for a multi-TeV linear e^+e^- collider using an innovative two-beam acceleration technique to achieve a high accelerating gradient, and CLIC 1 [2] is an essential step proposed at CERN in the R&D program toward CLIC. CLIC 1 would be based on one module of the eventual full CLIC accelerator, capable of delivering an intense, low-emittance e^- beam with an energy ~ 70 GeV. CLIC 1 is required to provide proof-of-principle for the two-beam acceleration mechanism of CLIC on a large scale, and would represent a major investment in engineering and other resources. It is natural to seek to maximize the physics return on this investment.

Several possible uses of an intense e^- beam are readily apparent. One could in principle use it for *fixed-target experiments*, for example. One could envision *colliding CLIC 1 with the LHC proton beam*, but the orientation and depth of CLIC 1 that would be required are not compatible with the possibility of extending CLIC 1 subsequently to become the full CLIC machine. If one had two CLIC 1 machines, a positron source and damping rings, one could make e^+e^- collisions. There has recently been a resurgence of physics interest in a new round of high-statistics experiments at the Z^0 peak, *GigaZ* [3–5], aimed at higher-precision electroweak measurements. The centre-of-mass energy range $\sim m_Z$ would certainly be within range of a pair of CLIC 1 machines, but effectiveness of the *GigaZ* program would require the positrons to be polarized, as well as the electrons, which is a technical challenge. There is also interest in returning to *the* $e^+e^- \to W^+W^-$ *threshold*, in order to measure m_W more precisely. The W^+W^- threshold would be within reach of a modest upgrade of the nominal CLIC 1 energy.

Alternatively, with two CLIC 1 machines, or even just one feeding two arcs à la SLC, and a laser backscattering facility to produce high-energy photons by the Compton process $e^-\gamma_{laser} \to e^-\gamma$. One could make $e^-\gamma$ *and/or* $\gamma\gamma$ *collisions* at centre-of-mass energies up to ~ 0.9 or $\sim 0.8 \times E_{CM}(e^-e^-)$, respectively. A polarized positron source would not be needed for such experiments. The principles of photon colliders [6] and the physics interest of $\gamma\gamma$ collisions, in particular, have been documented extensively [7,8].

Precision electroweak fits suggest [9] that the most likely mass for the Standard Model Higgs boson is just above the limit of 114 GeV provided by direct searches at LEP [10]. Moreover, the mass range $m_H \lesssim 130$ GeV [11] is suggested independently by supersymmetry. We also recall that the last days of LEP even provided a direct hint for a Standard Model-like Higgs boson with mass ~ 115 GeV [10], and that LEP could not exclude a supersymmetric Higgs boson as light as ~ 90 GeV. The possibility of such a light Higgs boson may be confirmed or refuted by the Tevatron collider within a few years, and the LHC would certainly measure the value of m_H. With the injection energy of 9 GeV, the nominal energy of CLIC 1 is 77 GeV. Therefore, the effective $E_{CM}(\gamma\gamma)$ could be tuned to a value up to $\sim 0.8 \times 154$ GeV ~ 120 GeV.

Thus there exists an opportunity for turning CLIC 1 into a Higgs factory, a proposal we term the CLIC Higgs Experiment, or CLICHE. As discussed in [12], the option of colliding the beams from two CLIC 1 machines looks promising, and the geometric e^-e^- luminosity may attain around 4.8×10^{34} cm^{-2}s^{-1}. Combined with a suitable laser backscattering system, such a luminosity would enable accurate measurements of the properties of the Higgs boson. For example, the laser system described below could yield a total $\gamma\gamma$ luminosity of up to 200 fb^{-1} per 'Snowmass year' of 10^7s, which could produce around 22,000 light Standard Model (SM) Higgs particles.

In subsequent sections of this paper, we first assemble some initial considerations of accelerator aspects of CLICHE, including the requirements for the CLIC 1 beam parameters and the laser system if one is to attain a luminosity sufficient to study Higgs physics. Then we review briefly some of the most interesting physics measurements possible with CLICHE, which could include accurate measurements of m_H, $\Gamma(H\to\gamma\gamma)\times\mathcal{B}r(H\to\bar{b}b)$, $\Gamma(H\to\gamma\gamma)\times\mathcal{B}r(H\to WW)$, $\Gamma(H\to\gamma\gamma)\times\mathcal{B}r(H\to\gamma\gamma)$, and the CP properties of the $H\to\gamma\gamma$ coupling. We study the capability of CLICHE to distinguish a Standard Model Higgs from the lightest Higgs boson in the minimal supersymmetric extension of the Standard Model (MSSM), and also discuss a more general two-Higgs-doublet model.

As we also mention, there are other physics processes that might be interesting at CLICHE, e.g., QCD reactions in $\gamma\gamma$ collisions and the reaction $e^-\gamma\to\nu W^-$ in $e^-\gamma$ collisions, which would provide an opportunity to measure m_W and Γ_W. We also advertise the physics opportunities for Higgs physics offered by higher-energy $\gamma\gamma$ colliders, for which CLICHE might serve as an engineering prototype. For example, the study of higher-mass Higgs bosons may best be done at high-energy $\gamma\gamma$ colliders, due to the fact that they are produced in the s channel (so that all of the phase space is available for producing the Higgs mass) [13, 14], and the fact that the photon beams can be produced in a state of definite CP.

2 Accelerator considerations

This section describes two important components of CLICHE, namely the CLIC 1 electron accelerator and the laser backscattering system.

At CERN, a high energy, high luminosity electron-positron linear collider (CLIC for Compact LInear Collider) is being studied as a possible post-LHC facility [1]. It is based on a novel two-beam scheme and uses high-frequency, high-gradient normal-conducting structures to accelerate the beam. The power to accelerate this main beam is obtained by decelerating drive beams in a dedicated beam line passing parallel to the main linac. CLIC requires two drive-beam complexes, each of which generate the 22 drive-beam pulses necessary to power 22 drive-beam decelerators for one of the two main linacs, for e^+e^- collisions at 3 TeV centre-of-mass energy. The two-beam acceleration has been demonstrated successfully in two test facilities (CTF1 and CTF2). A test of the drive-beam generation will take place at a new test facility (CTF3) [15], presently under construction. Its operation will enables one to judge whether the technology works, and it is expected that a conceptual design report for CLIC could be completed by the end of 2006. CTF3 should be followed by CLIC 1, which is conceived to provide a full scale test of beam dynamics and power handling.

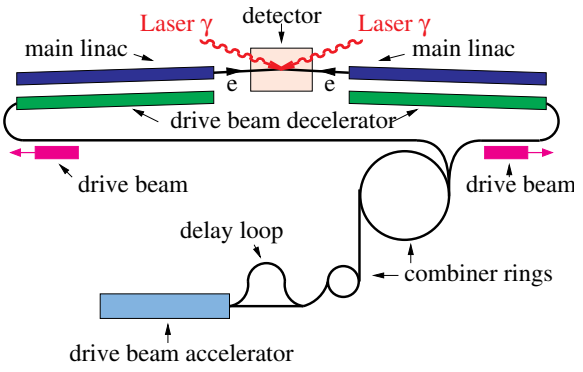

Fig. 1. Schematic sketch of a layout for a $\gamma\gamma$ collider based on CLIC 1

2.1 Parameters of CLIC 1

CLIC 1 is proposed to consist of one drive-beam generation complex and one drive-beam decelerator, with the corresponding length of main linac sufficient to accelerate a main beam by about 68 GeV.

Recently, an exploratory study has been carried out to determine how this facility could be turned into a collider with a high geometric e^-e^- luminosity, which could be used as the basis for a $\gamma\gamma$ collider [12]. This would require the addition of a small-emittance main-beam source and a final-focus system able to achieve small spot sizes at the interaction point (IP). In addition, it would be necessary to achieve a high beam current in the main linac. The main linac of CLIC 1 could in principle be turned into a collider by adding arcs as in SLC [16]. To limit the energy loss and emittance growth from synchrotron radiation, this would require very large arcs with many magnetic cells, resulting in increased complication and challenges for performance and cost. The other solution considered was to add a second CLIC 1 linac pointing at the first. Only this solution will be studied here, as it promises higher luminosities at similar or even reduced cost, if the long term investment is taken into account. The preliminary parameters of a potential e^-e^- collider are given in Table 1. A more detailed investigation is required in order to establish the feasibility of the approach and to identity possible further improvements.

In the proposed CLIC 1 collider scheme, the CLIC drive-beam complex can power both linacs. Alternate pulses are sent into the first and second linac, as seen in Fig. 1. The two pulses accelerate the main beams at the same time if the drive-beam complex is properly placed. The third pulse can be used to power again the first linac and the fourth to power the second, and so on, using all

Table 1. Example parameters for a CLIC 1 collider

variable	symbol	value
total power consumption for RF	P	150 MW
beam energy	E	75 GeV
beam polarization	P_e	0.80
bunch population	N	4×10^9
number of bunches per train	n_b	154
number of trains per rf pulse	n_t	11
repetition rate	$f_{\rm rep}$	100 Hz
rms bunch length	σ_z	30 μm
crossing angle	θ_c	≥ 20 mrad
normalised horizontal emittance	ϵ_x	1.4 μm
normalised vertical emittance	ϵ_y	0.05 μm
nominal horizontal beta function at the IP	β_x^*	2 mm
nominal vertical beta function at the IP	β_y^*	20 μm
e^-e^- geometric luminosity	$\mathcal{L}$	4.8×10^{34} cm^{-2}s^{-1}

drive-beam pulses. This effectively increases the repetition frequency from 100 Hz to 1.1 kHz. A repetition frequency of 200 Hz is foreseen for CLIC at a centre-of-mass energy of 500 GeV and further research and development is required to design structures that could tolerate the heat load of an increased repetition rate of up to 1.1 kHz as proposed here.

In the preferred two-beam scheme, the main beams would be generated by a conventional electron source, which could provide a polarization of about 80%. The injector could likely use the slightly modified SPS as a damping ring [17,18]. The beams would be accelerated to 9 GeV before injection into the main linac, increasing the maximum beam energy to $\sim$ 77 GeV. After the linac, a collimation system would scrape off the beam tails, and a final-focus system would focus the beams down to about 2.9 nm vertically and 154 nm horizontally.

The geometric e^-e^- luminosity at the full repetition frequency is $\mathcal{L} \simeq (4 \times 10^9 \times 4 \times 10^9/154 \times 10^{-7}/2.9 \times 10^{-7})(100 \times 11 \times 154/4/3.1415) = 4.8 \times 10^{34}$cm^{-2}s^{-1} (or $\mathcal{L} \simeq 0.9 \times 10^{34}$ cm^{-2}s^{-1} if the repetition frequency would remain at the design value for the 500 GeV CLIC of 200 Hz). On the other hand there may still be possibilities to increase the luminosity by other means like larger bunch charge or decreased vertical emittance. We therefore think it it is reasonable to base the estimates presented here on the luminosity obtained for the full repetition frequency.

2.2 Laser backscattering system

The photon beams required by CLICHE would be produced via the Compton backscattering of laser light off the high-energy electron beam from CLIC 1. The bunch-to-bunch distance and pulse length of CLICHE are of the same order of magnitude as those for NLC. The laser requirements for CLIC and NLC are therefore comparable, since they both use the Mercury technologies[1] - pump diodes, Yb-SFAP crystals, cooling, chirp pulse, etc. [7], the only differences being at the front end. On the other hand, the TESLA option [8] requires a high-speed lower-power optical switch (Pockels cell) which is under development at LLNL.

In the laser-beam collision at the conversion point, the maximum energy of the scattered photons is:

$$\omega_m = \frac{x}{x+1}E_0; \quad x \approx \frac{4E_0\omega_0}{m^2c^4} \simeq 15.3\left[\frac{E_0}{\rm TeV}\right]\left[\frac{\omega_0}{eV}\right], \quad (1)$$

where E_0 is the electron beam energy and ω_0 the energy of the laser photon. In connection with NLC studies [7], the case $E_0 = 250$ GeV, $\omega_0 = 1.17$ eV, i.e., $\lambda = 1.0$ μm, has been considered. This would correspond to $x = 4.5$ and $\omega_m = 0.82E_0$. In the case of CLICHE, the centre-of-mass energy of the accelerator would be $E_{CM}(e^-e^-) \simeq$ 150 GeV. In order for $E_{CM}(\gamma\gamma)$ to be close to the mass of a 115 GeV Higgs boson, the energy of the laser photon is chosen to be 3.53 eV instead of 1.17 eV, resulting in a maximum photon energy of roughly 60 GeV.

We need to add frequency multipliers to reduce the wavelength. The increase in the laser frequency is achieved by adding a tripler to the laser system. In this case it can be assumed that the 1.054 μm laser can be turned into one with 0.351 μm. As a consequence, the power provided by the photons is reduced by a factor 1/3. However the area of the focal spot is also reduced by 1/3, so the overall effect cancels out in the power in the peak. A 70% tripling efficiency is expected. It should be kept in mind that, the achievable spot size is determined by the size of the final focusing optic and the wavefront variation. When the light is tripled the wavefront tolerances become a factor of three tighter in order to achieve a diffraction limited spot. Parameters of the electron and laser beams are shown in Table 1 and 2. We find that CLICHE requires between $154 \times 2 \times 100 = 30800$ and $154 \times 11 \times 100 = 169400$ pulses/second. As a consequence, the use of more elaborate multi-pass optics than the two-pass system designed for NLC [7] would be important for reducing the required number of laser pulses.

The optimum polarization combination that we anticipate for the electron beam P_e and the laser beam P_L is $P_eP_L = -0.8$. In this case the generated photon spectrum peaks at its maximum energy, ω_m. In addition, the high-energy photon beam is almost completely polarized around the peak energy. In order to enhance the Higgs production and to suppress the background events, from $\gamma\gamma \to \bar{b}b + ng$ in particular, the polarizations of the colliding photon beams should be arranged so that $J_z = 0$ collisions dominate. With the CLIC 1 beam energy, the Higgs particle of 115 GeV is produced almost at rest, while the low-energy background events are strongly boosted. Hence the backgrounds will in general have topologies that are different from the desired signal events, as discussed later.

[1] This laser technology is capable of delivering the 10 kW of average power in short pulses of 1 TW peak power. The total energy of a pulse is 1 J

Table 2. Example of laser parameters for a $\gamma\gamma$ collider based on CLIC 1 for $\mathcal{L}_{ee} = 4.8 \times 10^{34}\mathrm{cm}^{-2}\mathrm{s}^{-1}$

variable	symbol	value
Laser beam parameters		
Wavelength	λ_L	0.351 μm
Photon energy	$\hbar\omega_L$	3.53 eV = 5.65×10^{-19} J
Number of laser pulses per second	N_L	$169400\,\mathrm{s}^{-1}$
Laser peak power	W_L	2.96×10^{22} W/m^2
Laser peak photon density		5.24×10^{40} photons/m^2/s
Photon beam		
Number of photons per electron bunch	N_γ	9.6×10^9
$\gamma\gamma$ luminosity	$\mathcal{L}_{\gamma\gamma}$	2.0×10^{34} cm^{-2}s^{-1}
$\gamma\gamma$ luminosity for $E_{\gamma\gamma} \geq 0.6E_{CM} = 90$ GeV	$\mathcal{L}_{\gamma\gamma}^{peak1}$	3.6×10^{33} cm^{-2}s^{-1}
$\gamma\gamma$ luminosity for $E_{\gamma\gamma} \geq 0.7E_{CM} = 105$ GeV	$\mathcal{L}_{\gamma\gamma}^{peak2}$	2.1×10^{33} cm^{-2}s^{-1}

The expected total energy spectra and polarization are shown in Fig. 2. The luminosity calculation assumes improvements over what was originally proposed in [12]:

- use of the most recent NLC Final-Focus System (FFS) for operation of the center-of-mass of 0.5-1 TeV [19],
- and increasing the strength of the bending magnets by a factor of 4.35, with corresponding decreases in the sextupole, octupole and decapole strengths by 4.35, 4.35^2 and 4.35^3. This allows the beta functions to be reduced from the NLC values: β_x=2 mm (previously 8 mm) and β_y=20 μm (previously 100 μm).

Tracking simulations of the FFS that take into account the synchrotron radiation in the dipoles and quadrupoles and the initial beam energy distribution from the linac as simulated with `DIMAD` [20] and `PLACET` [21] predict a geometric luminosity of 5.0×10^{34} cm^{-2}s^{-1} for 11 trains per rf pulse. The energy spread was assumed to be $\Delta E/E \sim 0.23\%$. The horizontal and vertical normalized emittances were taken to be 1.4×10^{-6} m and 5×10^{-8} m, respectively, and the RMS at the IP is 138.1 nm (2.6 nm) in the horizontal (vertical) plane. However, `DIMAD` predicts that the effective beam spot is larger, (154×2.9) nm^2. This is due to effects such as synchrotron radiation and the combination of chromaticity of the FFS and the electron beam energy spread. As a consequence, the luminosity is simulated to be 15% lower than the 'ideal' scenario. These effects are taken into account in the luminosity results shown in Fig. 2. Using the laser parameters described above, the $\gamma\gamma$ luminosity with a centre-of-mass energy above 0.6×150 GeV is about $3.6 \times 10^{33}\mathrm{cm}^{-2}\mathrm{s}^{-1}$, and the polarization $< \lambda\lambda' >$ at the peak is 0.94.

We have chosen the distance between the conversion point and the interaction point to be 1mm. Detailed studies indicate that the optimal value is 1.4 mm, which would yield a somewhat higher luminosity. On the other hand, there would be a reduction in luminosity if a more conservative beam spot size were assumed, so we consider the figures presented here quite representative.

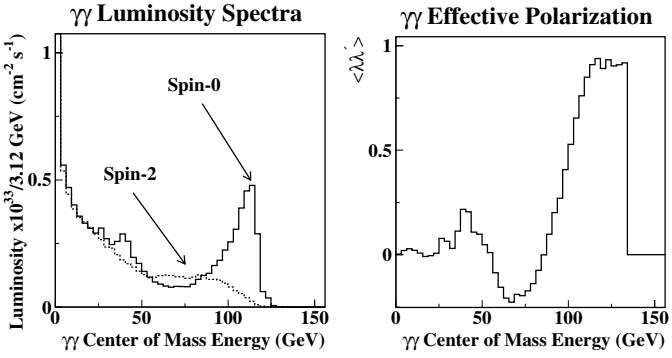

Fig. 2. Luminosity spectra and beam polarization as functions of $E_{CM}(\gamma\gamma)$ for the CLIC 1 parameters for 75 GeV electrons obtained with `DIMAD` [20] and `CAIN` [26] for $\mathcal{L}_{ee} = 4.8 \times 10^{34}\mathrm{cm}^{-2}\mathrm{s}^{-1}$

The laser-beam collision at the conversion point and the beam-beam collision at the interaction point have been simulated using `CAIN` [26] and using `GUINEA-PIG` [22]. The results of the two programs agree quite well. The luminosity spectra and the effective beam polarization as functions of $E_{CM}(\gamma\gamma)$ obtained using `CAIN` are shown in Fig. 2. Both of these need to be monitored and controlled accurately. At the E_{CM} under consideration, the spectra and luminosity can be measured using the reaction $\gamma\gamma \to e^+e^-$ [23]. The reaction $\gamma\gamma \to e^+e^-\gamma$ may also be useful for this purpose, but this requires further study. The polarization cannot be measured using the reaction $\gamma\gamma \to \mu^+\mu^-\mu^+\mu^-$ as originally suggested [23]. A promising way of measuring the photon polarization uses the reactions $e\gamma \to e\gamma$ and $e\gamma \to W\nu$. A detailed study of the second process in which the full photon energy spectrum is taken into account is in progress. Figure 3 displays the variation of the cross section with the photon polarization, together with the attainable statistical error. The latter would correspond to a determination of the photon polarization with a precision of $\pm1\%$.

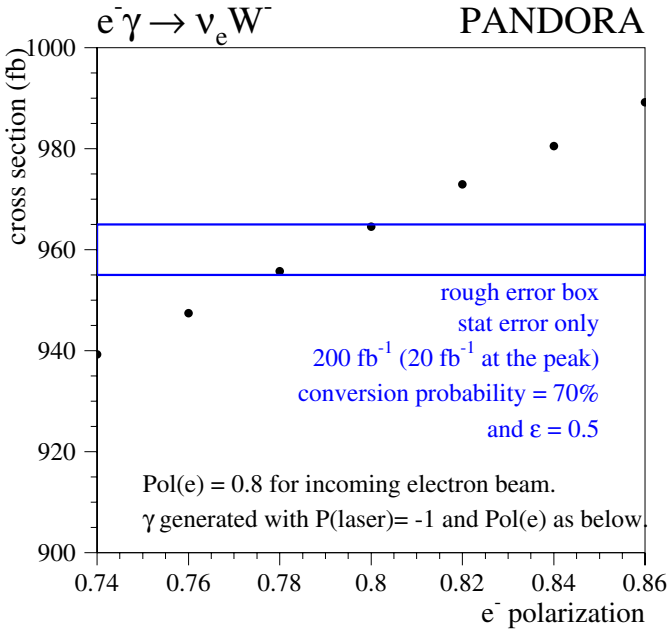

Fig. 3. The variation in the cross section for the $e\gamma \to W\nu$ process as a function of polarization. This analysis includes the full photon spectrum in the cross section calculation. The attainable statistical error in the cross-section measurement is also indicated

2.3 CLICHE for $E_{CM}(\gamma\gamma) > 115$ GeV

So far, we have only discussed parameters for $E_{CM}(\gamma\gamma)^{peak} \sim 115$ GeV. However, the $E_{CM}(e^-e^-)$ could be increased to provide $E_{CM}(\gamma\gamma)^{peak}$ in CLICHE of up to 2×68 GeV, if required by physics, such as a Higgs boson weighing 135 GeV. If the energy needs to be increased only slightly, one can think of using a single drive-beam decelerator per side, which is slightly longer than in the nominal CLIC scheme. The drive beam energy can be increased by installing more RF cavities, which allows the beam to power the longer decelerator. A straightforward way to increase further the energy would be to install one additional decelerator on each side. In this case, one could split the first RF pulse into two shorter ones feeding the first decelerator on each side. The second RF pulse would also be split to feed the second decelerator, and the following pulses would be used in a similar fashion. With this scheme the energy of the accelerator can be doubled while reducing the luminosity by a factor of 1.5. In contrast, simply running the accelerator at a slightly higher energy without changing the pulsing scheme would cost a factor 3 in luminosity.

3 Physics opportunities

Our primary thrust in this paper is to emphasize the Higgs physics accessible with CLICHE. However, there are other interesting physics opportunities, as we discuss in the last two subsections.

3.1 A Higgs factory

There have been many investigations of the physics possibilities of $\gamma\gamma$ colliders, including discussions of $\gamma\gamma$ options at JLC [24], NLC [7] and TESLA [8]. Here we describe results from exploratory studies of a $\gamma\gamma$ collider optimized for a light Higgs factory scenario at CLIC 1. As discussed in some detail below, several important measurements of Higgs properties can be made at a Higgs factory. In fact, for many of the analyses, running close to the Higgs threshold has important advantages.

We begin with a discussion of the Higgs production cross section. The excitation curve for a Higgs boson with mass around 115 GeV as a function of $E_{CM}(e^-e^-)$ for unpolarised electrons is shown in Fig. 4a. We see that the cross section rises rapidly for $E_{CM}(e^-e^-)$ between 140 and 160 GeV, providing a physics opportunity for CLIC 1 with a beam energy of 77 GeV, if indeed $m_H \sim 115$ GeV. Figure 4b shows the cross section as a function of Higgs mass for three choices of $E_{CM}(e^-e^-)$. We note that the excitation curve increases by a factor of three if the electron beams are 80% longitudinally polarized. The CLIC 1 energy could be somewhat lower if the lower limit of about 90 GeV on the lightest MSSM Higgs mass is saturated, whereas an energy upgrade would be required if the MSSM upper bound of about 130 GeV were to be saturated.

The most important decay modes of a Standard Model Higgs boson in the range between 100 and 200 GeV are shown in Fig. 5. We see that the $H \to \gamma\gamma$ coupling used to produce the Higgs boson at CLICHE yields a relatively minor decay mode, whereas the dominant decay mode for a Standard Model Higgs boson weighing $\sim$ 115 GeV is $H \to \bar{b}b$. Indeed, the most promising reaction at such a Higgs factory is $\gamma\gamma \to H \to \bar{b}b$, as we discuss below. Other decay channels accessible at CLICHE include $H \to WW$ and $H \to \gamma\gamma$. In the Standard Model, the branching ratios for $\mathcal{B}r(H \to b\bar{b})$, $\mathcal{B}r(H \to WW)$ and $\mathcal{B}r(H \to \gamma\gamma)$ for a Higgs mass of 115 GeV are: 73.7%, 8.8% and 0.2%, respectively. One of the objectives of CLICHE would be to test these predictions, and use measurements of them to distinguish between the Standard Model and its possible extensions, such as the minimal supersymmetric extension of the Standard Model (MSSM) or a more general two-Higgs-doublet model (2HDM), as we discuss later.

3.1.1 Higgs measurements with CLICHE

In all the studies shown below, realistic beam spectra and luminosities were used. The calculations were based on the `CAIN` program [26] which includes the non-linear effects that can cause distortions in the photon beam energy spectra, as well as the latest description of the interaction region. The photon helicities were taken into account in the signal and background estimations. The events were generated using `PANDORA-PYTHIA` [27,28], and `LCDROOT FASTMC` [29] was used for the detector simulations, including calorimeter energy smearing.

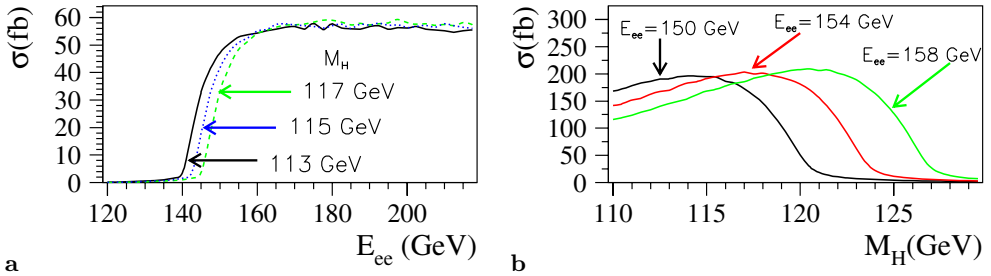

Fig. 4. a The cross sections for $\gamma\gamma \to H$ for different values of m_H as functions of $E_{CM}(e^-e^-)$ for unpolarised photons. **b** The cross section for $\gamma\gamma \to H$ as a function of m_H for three different values of $E_{CM}(e^-e^-)$. Here the electrons are assumed to be 80% polarized longitudinally, and the lasers circularly polarized, so that the produced photons are highly circularly polarized at their maximum energy. Non-linear effects are ignored in the production of the luminosity spectra used to obtain these results, and the cross section values are given with respect to the full $E(\gamma\gamma)$ energy range

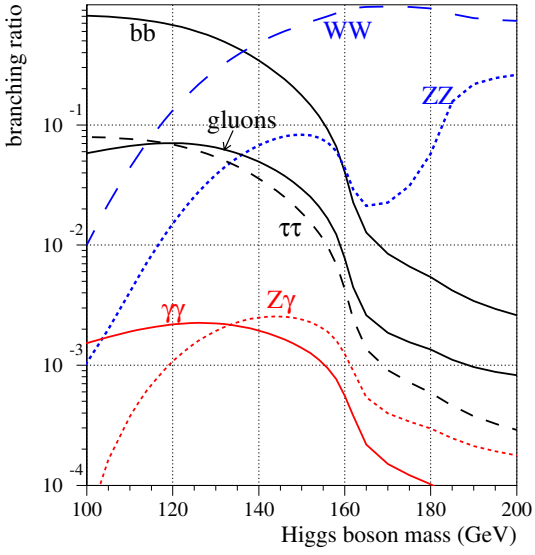

Fig. 5. The principal decay modes of the Higgs boson [25] in the mass range favoured by precision electroweak experiments

We give only a brief overview of exploratory results pertaining to the Standard Model Higgs boson with a mass in the range 110–125 GeV.

Mass

A special feature of the $\gamma\gamma$ collider is the sharp edge of the $\gamma\gamma$ luminosity function, as depicted in Fig. 2. The position of this edge can be controlled by changing the electron beam energy. As it sweeps across the threshold for Higgs production, the number of, e.g., $\bar{b}b$ events will increase dramatically. This phenomenon is already reflected in the sharpness of the excitation curves of Fig. 4. Since the position of this turn-on depends on the Higgs mass, a threshold scan offers the possibility to measure the Higgs mass kinematically, as developed in [30].

To study the sensitivity to the Higgs mass, we define a simple figure of merit to quantify the difference in yields for two different assumed Higgs masses at a given e^-e^- centre-of-mass energy: $F = |N_1 - N_2|/\sqrt{\sigma^2_{N_1} + \sigma^2_{N_2}}$.

As shown in Fig. 4, there is a point of optimum sensitivity to the Higgs mass a few GeV below the peak of the cross section. The raw number of events at a single energy cannot be used to measure the mass, however, because the $\gamma\gamma$ partial width cannot be assumed known *a priori*. There is another point, though, close to the maximum of the cross section, at which there is no sensitivity to the Higgs mass, and with maximum sensitivity to $\Gamma_{\gamma\gamma}$, allowing the separation of these two quantities. These points are illustrated in Fig. 6. Furthermore, the background can be estimated using data obtained by running below the threshold. To estimate the sensitivity of the yields to m_H, we work with a simple observable based on the ratio of background-subtracted yields at peak and at threshold:

$$Y = \frac{N_{\text{peak}} - N_{\text{below}} \cdot r_p}{N_{\text{threshold}} - N_{\text{below}} \cdot r_t}$$

where N is the number of events in a mass window logged at the peak, on the threshold, and below threshold, and r_p and r_t are scale factors to relate the background data taken below threshold to the expectation at peak and at threshold. We have propagated statistical uncertainties, and, assuming one year of data on peak, half a year on threshold and another half below threshold, we find $\sigma_Y/Y = 0.088$. This translates into an error on the inferred Higgs mass of 100 MeV. A more refined treatment should improve this estimate somewhat. This estimate is obtained using the laser and beam energies proposed for CLIC 1 and the analysis results shown in Fig. 7. It is still necessary to investigate how sensitive the luminosity function is to the shape of the luminosity curve. It is not sensitive to the electron polarization precision.

$H \to \bar{b}b$

Due to the large branching ratio for $H \to \bar{b}b$ decay for a Higgs mass $\sim$ 115 GeV, this is the main channel for Higgs studies at CLICHE. This channel has received the most attention and the studies are already quite detailed [14,32,33]. Our analysis includes perturbative QCD backgrounds, including $\gamma\gamma \to \bar{b}b(g)$ and $\gamma\gamma \to \bar{c}c(g)$. The $\bar{q}q$ backgrounds are suppressed by choosing like polarizations

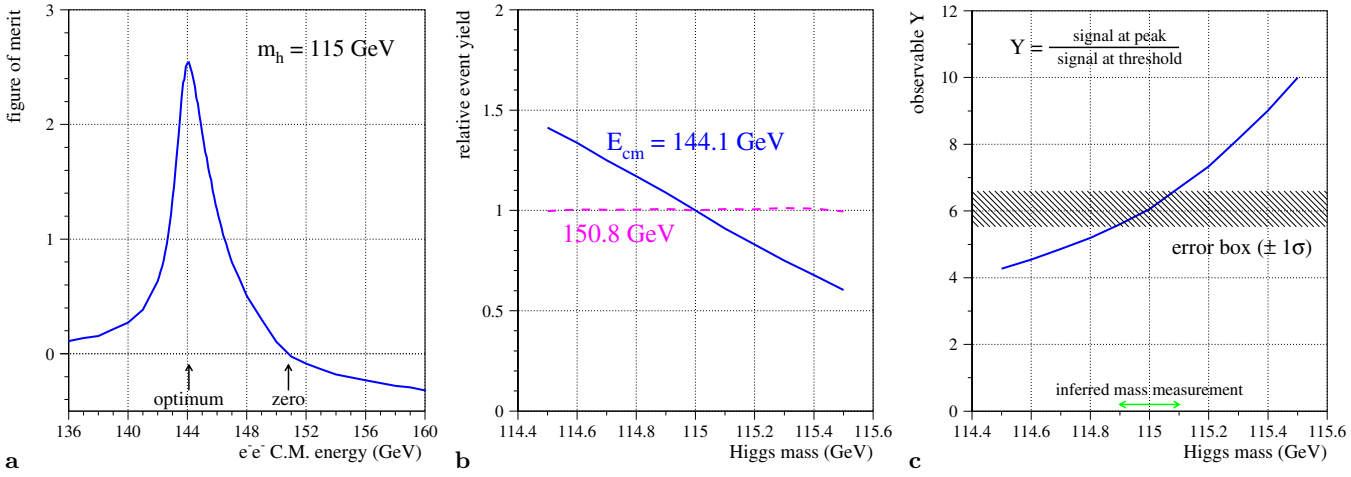

Fig. 6. a A figure of merit quantifying the measurement error on the mass as a function of the e^-e^- centre-of-mass energy. The optimum and zero sensitivity points are marked. **b** Relative yield for a 115 GeV Higgs boson at the point of optimum sensitivity and zero sensitivity to m_H. **c** Behavior of the observable Y as a function of m_H, and the projected error

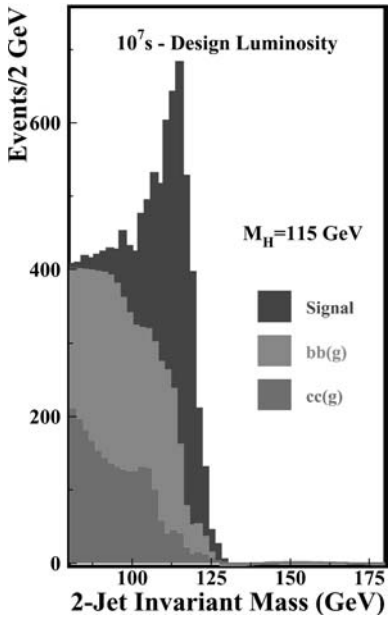

Fig. 7. Observability of the $H \to \bar{b}b$ decay mode for m_H = 115 GeV, with CLICHE running so that the peak $E_{CM}(\gamma\gamma)$ = 115 GeV. The background shown *includes* the correction for the deficiancy in the NLC approximation of PYTHIA [27]

for the colliding photons, but this suppression is not so strong when the final states contain additional gluons.

In this analysis we used the Durham jet algorithm and imposed a cut at $y = 0.02$ to define the two jets. The main cuts are: (1) only two-jet events are accepted, (we do not find any improvement if we include three-jet events as well), (2) $|\cos\theta_J| < 0.5$, which is 50% efficient, and (3) the two jets are required to be back-to-back, specifically, we require $|p_{x1}+p_{x2}|$, $|p_{y1}+p_{y2}|$, $|p_{z1}+p_{z2}| < 12$ GeV for the two jet momenta. The last cut is very important for the background suppression, but at a significant cost in the signal. The efficiency of this cut is 85-90% for the 33% of events that do not contain neutrinos, but there is significant reduction in efficiency for the rest of the events. We assume here that there will be a 3.5% $c\bar{c}$ contamination and that the b tagging is 70% efficient for double tagging [4]. One-third of the two-jet events have no neutrinos from semileptonic b or c decays, and 85% of these pass the 'back-to-back' requirement. The other two-jet events pass with a 55% efficiency. Given acceptances of 50% for the $\cos\theta_J$ requirement, and 90% for the two-jet requirement, the overall efficiency is 20%.

The signal and background distributions after all cuts are shown in Fig. 7. The spin-2 contribution dominates the surviving background. Initial studies indicate that the NLO approximation employed by PYTHIA [27] underestimates the spin-2 background by 10%, the spin-0 background by a factor of 10 and the combined sample by 30% relative to the calculation in [33]. The background shown in Fig. 7 *includes* the correction for the deficiency in the NLO approximation of PYTHIA.

Recent photoproduction measurements of the b cross section at the highest energies at LEP are larger than predictions from NLO perturbative QCD calculations. L3 [34] and OPAL [35] report values for the cross section of $ee \to ee b\bar{b}X$ at $E_{CM}(e^+e^-) = 194$ GeV which are, respectively, $3\,\sigma$ and $2.5\,\sigma$ larger than predicted. Hadronic final states containing b quarks are identified by detecting leptons from their semi-leptonic decays. The effective $\gamma\gamma$ center of mass energy at which these measurements are made is considerably lower than the one at CLICHE, and it is therefore not clear that this will affect the signal-to-background ratio, in particular after all selection cuts made. This background can be controlled by measuring off the Higgs mass peak.

The mass resolution is around 6 GeV with a jet energy resolution of $\sigma_E = 0.3 \times \sqrt{E}$. The distribution in the di-jet invariant mass, m_{jets}, for a $m_H = 115$ GeV Higgs found in this study with an integrated luminosity of 200 fb^{-1} is shown in Fig. 7. A clear signal peak can

be seen above sharply falling backgrounds. Including the bins above $m_{jets} = 100\,(110)$ GeV, we obtain 3280 (2310) signal events and 2430 (875) background events. Thus, the signal-to-background ratio is expected to be 3/2 (3/1) after all cuts.

Our studies have not yet incorporated backgrounds that might arise as the result of the resolved photon processes in which a quark or gluon constituent of one of the back-scattered photons is responsible for initiating a background process that creates a pair of high-p_T b or c jets. Such additional scattering primarily yield additional low-p_T jets that would underlie the $b\bar{b}$ jets arising from Higgs production. They would thus make it less efficient to isolate the true 2-b-jet signal using cuts that require exactly two reconstructed jets which are rather precisely back-to-back. Mass resolution could also deteriorate, as might the efficiency for b-tagging. The level of this background is, of course, determined by the number of bunch crossings over which the detector integrates. The bunch structure of CLIC leads to a bunch crossing every 0.67 nanoseconds. The detector components will generally not have the capability to time-stamp hits with this resolution and will provide information integrated over several bunch crossings. Hence an R&D program on the development of fast detectors will need to be pursued in the coming years (this is also the case for detectors at the NLC, where the separations between bunches are only a few nanoseconds). The components most likely to determine the total number of bunch crossings that will be integrated over, for the studies of interest here, will be the silicon pixel detectors, for which a time-stamping capability of 25 nsecs has been demonstrated for LHC experiments. It can be expected that this resolution will improve perhaps to 10 nsec or even 5 nsec within the next 10 years, based on present ideas that still need to be tested. Nevertheless, this means that of order 10 bunch crossings will contribute to measured events at CLICHE, which will affect the background shape of Fig. 7. Initial studies have shown that the Higgs signal deteriorates only slightly.

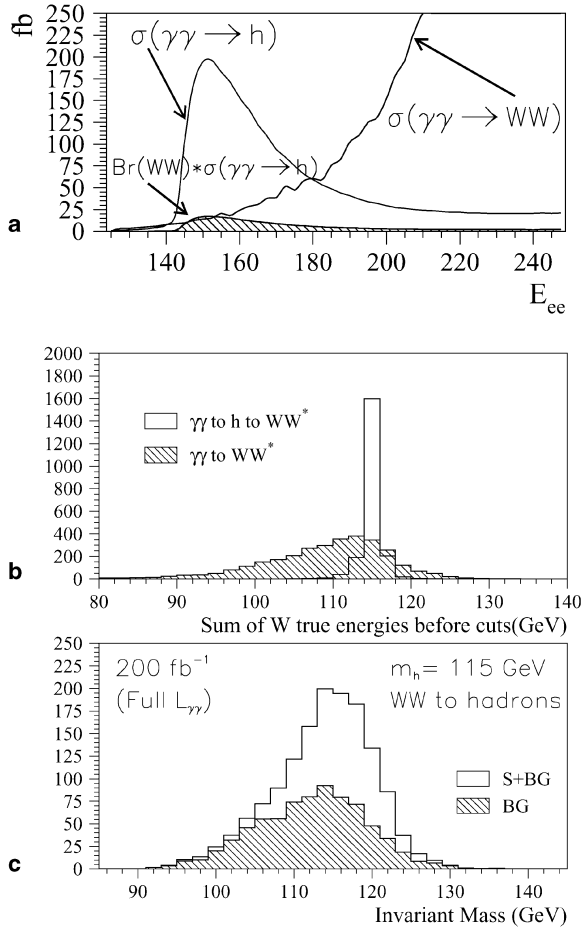

Fig. 8. a Cross sections for $\gamma\gamma \to h$, $\gamma\gamma \to h \times \mathcal{B}r(h \to WW)$ for $m_H = 115$ GeV and $\gamma\gamma \to WW$ production. The electrons are assumed to be 80% polarized and the laser to be circularly polarized. **b** Comparison of the ideal invariant mass of the WW pairs from signal and background events. **c** Selection of the WW decay mode of the Higgs boson for $m_H = 115$ GeV, running at $E_{CM}(\gamma\gamma) = 115$ GeV at CLICHE

$H \to WW$

Observation of this decay mode is extremely difficult at high-energy $\gamma\gamma$ colliders, because of the large cross section for W pair production. If the $\gamma\gamma$ centre-of-mass energy is below the W^+W^- threshold, however, the continuum production of W pairs is greatly reduced, allowing the observation of resonant production through a Higgs boson. The sharp peak in the $\gamma\gamma$ luminosity function seen in Fig. 2 plays a key role here. Figure 8a compares the cross sections for the continuum W pair production with the Higgs resonance curve. As shown, the cross sections for $\sigma(\gamma\gamma \to W^+W^-)$ and $\mathcal{B}r(h \to W^+W^-) \times \sigma(\gamma\gamma \to h)$ are comparable, if $E_{CM}(e^-e^-) = 150$ GeV for a $m_H = 115$ GeV. One significant difference between the two type of events is the energy distribution of the W^+W^- pairs, as illustrated in Fig. 8b.

Our study is concentrated on the hadronic decays of the W pairs. Jets are reconstructed using the Durham algorithm with $y = 0.003$. Four or more jets are required, each with $|\cos\theta_J| < 0.9$ to ensure a good measurement of the energy and direction of the jet. (These basic jet requirements differ from those of the $h \to b\bar{b}$ analysis.) The sum of the longitudinal momentum components of the jets must be less than 10% of the maximum $\gamma\gamma$ energy $E_{\gamma\gamma}^{\max}$. We first find the pair of jets with an invariant mass closest to m_W, which we call m_{12}, and we call the mass of all the remaining jets $m_{\rm other}$. The jet masses from $h \to WW^*$ saturate the phase space more than those from the continuum, so we require -10 GeV $< E_{\gamma\gamma}^{\max} - (m_{12} + m_{\rm other}) < 20$ GeV. This cut is useful against QCD multijet production ($\gamma\gamma \to q\bar{q}g$).

In contrast to the LHC, a $\gamma\gamma$ collide produces mainly W pairs of the same polarization, i.e., $W_L\,W_L$ and $W_T\,W_T$ but not $W_L\,W_T$. Also, the $J = 2$ contribution is much smaller than the $J = 0$ contribution. Consequently, the angular distributions of jets from continuum W pair production are very similar to those from $h \to WW$, and

no simple cut is helpful for enhancing the signal over the background.

After these selection criteria, 29% of the signal remains, and the signal-to-background ratio is 1.3. Figure 8 shows the invariant mass of all jets after these cuts, for signal and background. The shapes are very similar, so this signal measurement consists of event counting and subtracting the contribution from backgrounds. After one year, the expected statistical precision would be 5%. The other event topologies (two leptons and missing energy, or one lepton, missing energy and jets) remain to be studied. Techniques similar to those described in [36] may be used. We also believe that the channels $h \to ZZ, Z\gamma$ will be interesting, despite their relatively small branching ratios.

$H \to \gamma\gamma$

In almost any phenomenological context, the decay $H \to \gamma\gamma$ is a rare one. However, the number of Higgs events is large at a $\gamma\gamma$ collider, so an interesting number of $H \to \gamma\gamma$ events would be produced. Furthermore, the background from continuum $\gamma\gamma \to \gamma\gamma$ is small, since it is mediated by a fermion box. This background is sharply peaked in the forward direction, and it falls rapidly with $M_{\gamma\gamma}$.

A study of this channel has been completed [31]. Good calorimetry such as that planned for the CMS experiment allows for a very narrow mass peak from $H \to \gamma\gamma$. A cut on the angle of the photons with respect to the beam reduces the background significantly: $|\cos\theta_\gamma| < 0.85$ is optimal. Within a window of ± 2 GeV around the Higgs mass, a signal-to-background ratio of 1.3 is obtained. If CLICHE were run for one year at optimal conditions for the signal, 40 signal and 32 background events would be expected. Allowing for a 10% uncertainty on the background level, the signal would be measured to approximately 22%. After three years, the error would be as small as 12%.

The cleanliness of these events and good energy resolution in the electromagnetic calorimeter allow for an independent measurement of the Higgs mass. For a calorimeter of the CMS type, an accuracy of 60–90 MeV would be expected, depending on the total running time.

Other channels

A preliminary assessment of the $H \to \bar{c}c$ channel at a $\gamma\gamma$ collider is not very encouraging: relative to the $\bar{b}b$ mode, the $\bar{c}c$ signal is suppressed by factor of $(m_c/m_b)^2 \sim 1/10$, and the background is enhanced by a factor $(Q_c/Q_b)^4 = 16$. There is similar pessimism concerning the observability of $H \to gg$ and $H \to \tau^+\tau^-$.

Combining channels

A good measurement of the two-photon partial width, $\Gamma_{\gamma\gamma}$, is very important as it receives direct contributions from all charged massive particles, and there is no tree-level contribution. Since the Higgs production cross section is proportional to $\Gamma_{\gamma\gamma}$, the measurement of any yield provides information, in principle, on $\Gamma_{\gamma\gamma}$. Similarly, the total Higgs width might be used to distinguish a light Higgs in the Standard Model and in the MSSM. Information from the $H \to \bar{b}b$ and $H \to \gamma\gamma$ channels can be combined from measurements from an e^+e^- collider to obtain $\Gamma_{\gamma\gamma}$ and $\Gamma_{\rm total}$.

Table 3. The statistical errors on selected decay modes of a 115 GeV Higgs boson in the Standard Model. The $\gamma\gamma \to h$ cross section for the full (peak) $\mathcal{L}_{\gamma\gamma}$ given in Table 2 is 112 (624) fb. The expected yield for 200 (36) fb^{-1} is 22,400 Higgs particles

decay mode	raw events/year	S/B	ϵ_{sel}	$\mathcal{B}r$	$\Delta\Gamma_{\gamma\gamma}\mathcal{B}r/\Gamma_{\gamma\gamma}\mathcal{B}r$
$\bar{b}b$	16509	2.0	0.20	73.7%	2%
W^+W^-	1971	1.2	0.32	8.8%	5%
$\gamma\gamma$	47	1.3	0.85	0.23%	22%

From the study of the channel $H \to \bar{b}b$ we estimate a precision of 2.0% on the quantity $\Gamma_{\gamma\gamma} \times \mathcal{B}r(H \to \bar{b}b)$. There are methods for measuring the branching ratio $\mathcal{B}r(H \to \bar{b}b)$ to about 1.5% at an e^+e^- linear collider [7, 3]. By combining the information from both colliders, $\Gamma_{\gamma\gamma}$ can be inferred to a precision of 2.2%, to be contrasted with a 19% measurement from 500 fb^{-1} at TESLA (without the $\gamma\gamma$ option), for example.

Independent information on $\Gamma_{\gamma\gamma}$ comes from the $H \to \gamma\gamma$ channel. The number of events produced in this channel is proportional to $\Gamma^2_{\gamma\gamma}/\Gamma_{\rm total}$. The quadratic dependence on the $H \to \gamma\gamma$ partial width is interesting, because if $\Gamma_{\rm total}$ could be measured elsewhere or if a value from theory were assumed, a small error on $\Gamma^2_{\gamma\gamma}$ would be obtained, perhaps on the order of 6–7% if CLICHE is operated for three or more years.

The resolution on $\Gamma_{\gamma\gamma}$ from these two methods is plotted in Fig. 9 as a function of the integrated luminosity. The result is much better than what can be obtained from an e^+e^- collider alone.

As shown in Fig. 10, the $\Gamma_{\gamma\gamma}$ partial width in the MSSM can deviate a lot from the SM value; even for a fixed Higgs mass of 115 GeV, for example, a factor of two variation is possible. Note that this impacts the cross section and hence precision on the inferred value for $\Gamma_{\gamma\gamma}$. Nonetheless, it is clear that a precision of 2–6% would be very discriminating in the context of an unconstrained MSSM.

For some choices of MSSM parameters, the Higgs total width can be increased significantly over the Standard Model expectation. It is possible to extract a model-independent value for $\Gamma_{\rm total}$ by taking the measurement of the yield in the $\bar{b}b$ channel at a $\gamma\gamma$ collider and combining it with measurements of the Higgs branching ratios to $\bar{b}b$ and $\gamma\gamma$ from an e^+e^- collider:

$$\Gamma_{\rm total} = \frac{\{\Gamma_{\gamma\gamma} \times \mathcal{B}r(H \to \bar{b}b)\}}{\{\mathcal{B}r(H \to \gamma\gamma)\} \times \{\mathcal{B}r(H \to \bar{b}b)\}}. \qquad (2)$$

According to [7,3,37], the anticipated precision on $\mathcal{B}r(H \to \bar{b}b)$ and $\mathcal{B}r(H \to \gamma\gamma)$ are 1.5% and 19%, respectively. Combined with a precision of 2% on the numerator, this leads to a precision of about 20% for $\Gamma_{\rm total}$.

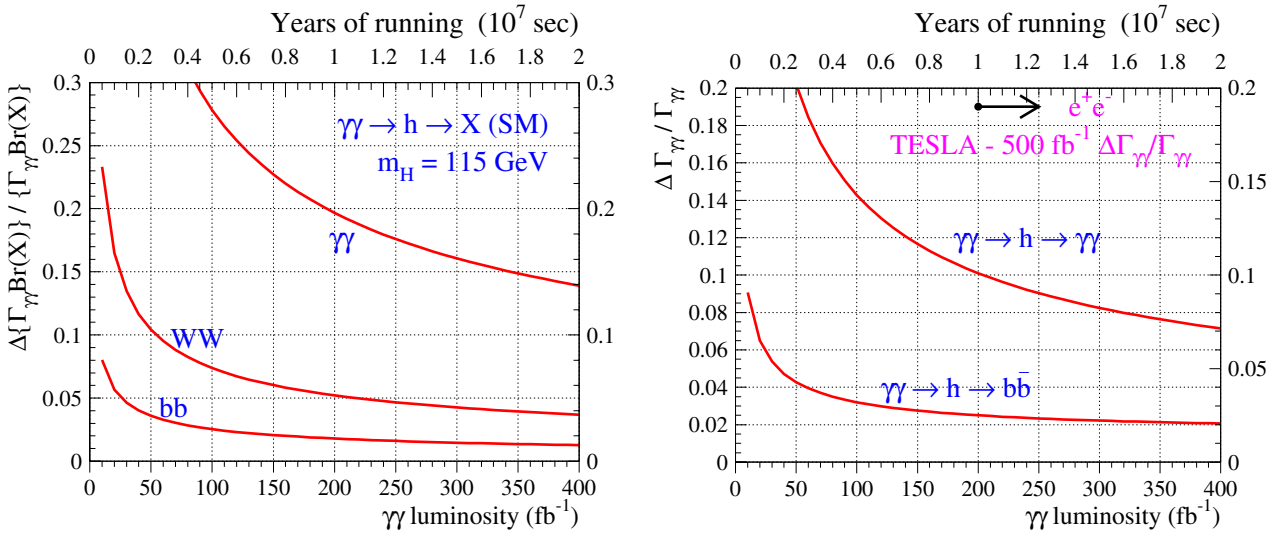

Fig. 9. *Left:* the precision on the yields for $H \to \gamma\gamma$, WW and $\bar{b}b$ as a function of integrated luminosity, or equivalently, running time. *Right:* the precision on the partial width $\Gamma_{\gamma\gamma}$ obtained from the $H \to \gamma\gamma$ and $\bar{b}b$ channels, when combined from information from an e^+e^- collider (see text for details). The precision is much better than that obtained from an e^+e^- collider alone

An independent value for $\Gamma_{\rm total}$ can be obtained on the basis of the yield for $H \to \gamma\gamma$. As discussed above, the partial width $\Gamma_{\gamma\gamma}$ could be known to 2.2% accuracy by combining the yield for $\gamma\gamma \to H \to b\bar{b}$ with a measurement of $\mathcal{B}r(H \to b\bar{b})$ from an e^+e^- collider. In this case, the signal measurement in the $H \to \gamma\gamma$ channel translates directly into a measurement of the total width, at an accuracy in the range 12–22%, depending on running time.

CP

A measurement that might be unique for $\gamma\gamma$ collider experiments like CLICHE could be that of the CP properties of the $H \to \gamma\gamma$ vertex [38], which can be measured by colliding photons with orthogonal linear polarizations, which define initial states of definite CP. In the Standard Model, the $H \to \gamma\gamma$ vertex has only a CP-even part, but in extended models, such as supersymmetry, there may also be a CP-odd part, which could provide an interesting window on the mystery of CP violation. The CP properties of the $H \to \gamma\gamma$ vertex are in principle distinct from those of other Higgs vertices, and hence have independent interest. This measurement would require higher-energy electrons and producing the photons using lasers of longer wavelength in order to reduce the interference and obtain a state with CP better defined [39,14].

Another window on the CP nature of the Higgs boson is provided by angular distributions in the $H \to W^+W^-$ channel [40]. This channel is useful because information can be obtained even in the absence of linearly-polarized photon beams. The accuracy on the asymmetry in the case of no background will be $\sqrt{(1-A^2)/N}$, where A is the measured asymmetry and N are the number of events. However in our case after two years of data taking, we estimate $\delta A/A \sim 5\%$ instead of 1-3% because the expected the signal to background ratio is 1.3.

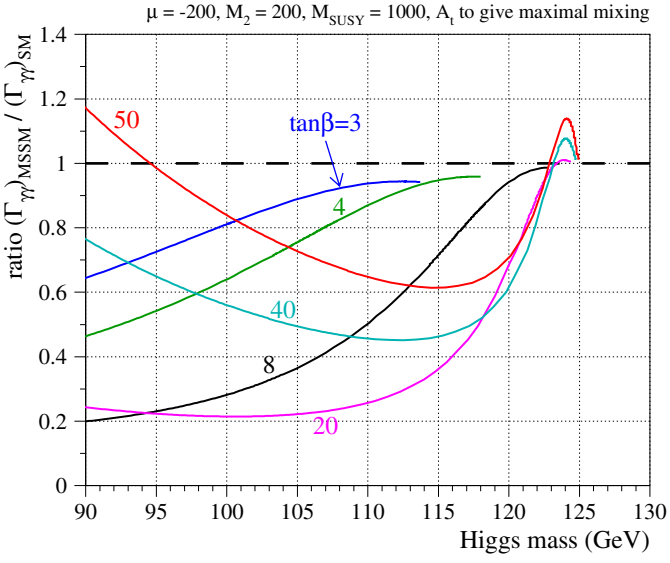

Fig. 10. The ratio of the partial width $\Gamma_{\gamma\gamma}$ in the MSSM to that in the SM [25]. The 'maximal mixing' [43] scenario has been chosen for this illustrative plot; this scenario tends to give the largest Higgs masses for a given $\tan\beta$ and M_A. These curves do not necessarily map out the largest possible variation in this ratio, nor have they been constrained by negative searches for Higgs bosons. The ratio of cross sections follows the same curves

Summary

We have briefly discussed measurement possibilities in the $\bar{b}b$, W^+W^- and $\gamma\gamma$ channels. The observability and statistical errors of the products $\sigma(\gamma\gamma \to H) \times \mathcal{B}r(H \to X)$ for

each of these decay modes are summarized in Table 3. Preliminary studies indicate that the systematic errors, *e.g.*, those due to the luminosity and polarization uncertainties, could be controlled to the same level. Thus it seems possible to measure $\sigma(\gamma\gamma \to H \to \bar{b}b, WW, \gamma\gamma)$ with overall precisions of 2, 5, 11%, respectively (see Fig. 9).

In addition, the Higgs mass can be measured three ways (fitting the peaks in the $\bar{b}b$ and $\gamma\gamma$ mass distributions, and by the threshold method), and the partial width $\Gamma_{\gamma\gamma}$ can be extracted on the basis of a measurement of $\mathcal{B}r(H \to \bar{b}b)$ from an e^+e^- collider to very good accuracy, not matched by any other method. Finally, possible CP asymmetries could be measured with a precision of about 5%.

3.1.2 Complementarity with other machines

Each of the combinations $\Gamma(H \to \gamma\gamma) \times \mathcal{B}r(H \to \bar{b}b, WW, \gamma\gamma)$ measurable at CLICHE is distinct from the quantities observable previously at the Tevatron: $\Gamma(H \to W^+W^-) \times \mathcal{B}r(H \to \bar{b}b)$, and the LHC: $\Gamma(H \to gg) \times \mathcal{B}r(H \to \gamma\gamma)$ and $\Gamma(H \to \bar{t}t) \times \mathcal{B}r(H \to \bar{b}b)$. It is estimated that the Tevatron observable could be measured with a precision of 20% and the LHC observables with precisions $\sim 7, 10\%$, respectively. The CLICHE measurement of $\Gamma(H \to \gamma\gamma) \times \mathcal{B}r(H \to \bar{b}b)$ would therefore be complementary to, and of higher accuracy than, these previous measurements, whilst the other CLICHE measurements would also be competitive.

At an e^+e^- collider like TESLA, the raw number of Higgs particles to be produced for $m_H = 120$ GeV, if we take into account the contribution from Higgsstrahlung and WW-fusion, is is 46,750 (50,320) per year at 350 (500) GeV. This is assuming that the TESLA design luminosity is $2.5\,(3.4) \times 10^{34}\mathrm{cm}^{-2}\mathrm{s}^{-1}$ at 350 (500) GeV. An e^+e^- collider would be able to measure with high precision $\Gamma(H \to ZZ)$ and all the dominant decay branching ratios $H \to \bar{b}b, \bar{c}c, gg, \tau^+\tau^-$ shown in Fig. 5. Moreover, such an e^+e^- collider could also be configured as a $\gamma\gamma$ collider, if it is equipped with a laser backscattering facility. This possibility is envisaged in the current designs of the JLC [24], NLC [7] and TESLA [8], but may not be scheduled for the initial phases of these machines.

At CLICHE, one could have 150 fb^{-1} in a year with $E_{CM}(e^-e^-) = 150$ GeV and a $\gamma\gamma$ centre-of-mass energy peaked at 115 GeV. We recall that a 115 GeV Higgs would be produced as an s-channel resonance, and that the event yield is estimated to be around 22,000 per year. Similar yields could be expected for $m_H \leq 125$ GeV (see Fig. 4b), if the extra energy was made available.

3.1.3 Discriminating between Higgs models using CLICHE measurements

Since the $H \to \gamma\gamma$ vertex is due to loop diagrams, it is sensitive to physics beyond the direct physics reach of CLICHE. For example, a 3% measurement of $\Gamma(H \to \gamma\gamma)$ would provide indirectly a 6% measurement of $\Gamma(H \to \bar{t}t)$, in the absence of new physics [41]. However, supersymmetry is a prime example of possible new physics that could influence the $H \to \gamma\gamma$ vertex, as seen in Fig. 10.

As an example how the precision achievable with CLICHE could help distinguish between models of Higgs bosons, in the following we compare Higgs production in $\gamma\gamma$ collisions in the Standard Model and its minimal supersymmetric extension, the MSSM. We do this by calculating the product of the production cross section and branching ratio for the lightest MSSM Higgs boson, h, normalized to the corresponding Standard Model value, with M_H set to the mass of the lightest MSSM Higgs, m_h:

$$R_{b,W,\gamma} := \frac{\left[\Gamma(\gamma\gamma \to h) \times \mathcal{B}r(h \to b\bar{b}, WW^*, \gamma\gamma)\right]_{\mathrm{MSSM}}}{\left[\Gamma(\gamma\gamma \to H) \times \mathcal{B}r(H \to b\bar{b}, WW^*, \gamma\gamma)\right]_{\mathrm{SM}}} \,. \tag{3}$$

Regions of the MSSM parameter space with strong deviations from the Standard Model are identified in the following. Strong suppression of these ratios could occur in problematic corners of the MSSM parameter space, where a specific decay channel or even MSSM Higgs production itself is inaccessible. The evaluation of the Higgs boson sector has been performed with the codes `FeynHiggs` [42], based on [43], and `Hdecay` [25].

In Figs. 11–13, the unconstrained MSSM is analyzed in three benchmark scenarios [44], originally proposed in connection with Higgs searches at LEP. The '$m_h^{\max}$' scenario maximizes the m_h value for a given $M_A, \tan\beta$ combination at fixed M_{SUSY} and m_t. The 'no-mixing' scenario has the same parameters as the $m_h^{\max}$ scenario, but no scalar top mixing. Contrary to [44], we have set $M_{SUSY} = 1500$ GeV and $m_{gl} = 1000$ GeV so as to increase the m_h values. In the last scenario, the value of μ is chosen to be large: $\mu = 1$ TeV. Contrary to [44], we have again set $M_{SUSY} = 1000$ GeV so as to increase the m_h values. The limits of LEP Higgs searches have been applied in these figures, using an updated version of the results as presented in [45]. However, the 'no-mixing' and 'large μ' scenarios have $m_h \lesssim 120$ GeV for the shown parameter space, whereas the $m_h^{\max}$ scenario results in $m_h \gtrsim 125$ GeV for large parts of the parameter space, which is at the limit of the reach of CLICHE. An analysis of similar scenarios for a TeV-class e^+e^- linear collider can be found in [46].

In Fig. 11, R_b is shown in the $M_A, \tan\beta$ plane. As expected, due to the enhanced $hb\bar{b}$ coupling, R_b is enhanced in most part of the parameter space in all three benchmark scenarios. Suppression only occurs for very small values of M_A: $M_A \lesssim 130$ GeV or small $\tan\beta$, $\tan\beta \lesssim 5$. Deviations from the Standard Model at the 3-5σ level can be observed up to $M_A \lesssim 300 - 500$ GeV, depending on the scenario. We note deviations from the Standard Model at the 1σ level in nearly the whole plane in the $m_h^{\max}$ scenario and up to $M_A \lesssim 500 - 600$ GeV in the other scenarios. These sensitivities are in the same ballpark as for a linear e^+e^- collider [46]. Thus, a $\gamma\gamma$ collider could offer a complementary method of distinguishing the MSSM from the SM in the Higgs sector.

Figures 12 and 13 show R_W and R_γ, respectively, for the three benchmark scenarios. As one would expect from

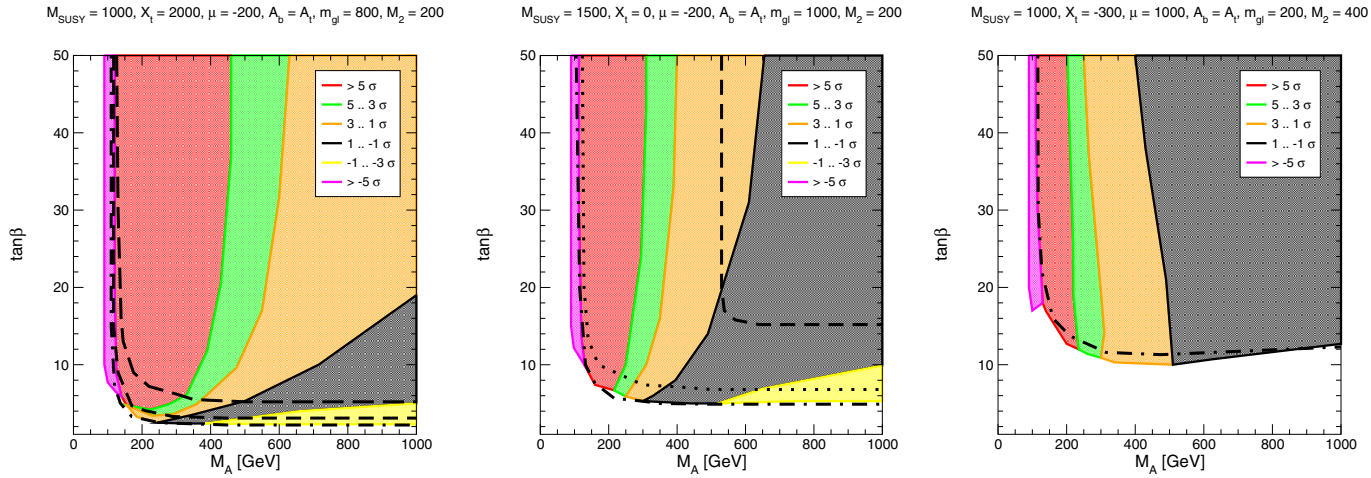

Fig. 11. The ratio R_b is shown in the $M_A, \tan\beta$ plane for the three benchmark scenarios described in the text. The observable deviation from the Standard Model is indicated for a 2% experimental precision in R_b. The contours for the corresponding Higgs masses are also included. Dot-dashed for 113 GeV, dotted for 115 GeV, dashed for 117 GeV and long dashed for 125 GeV (Not all lines are necessarily appear in all plots)

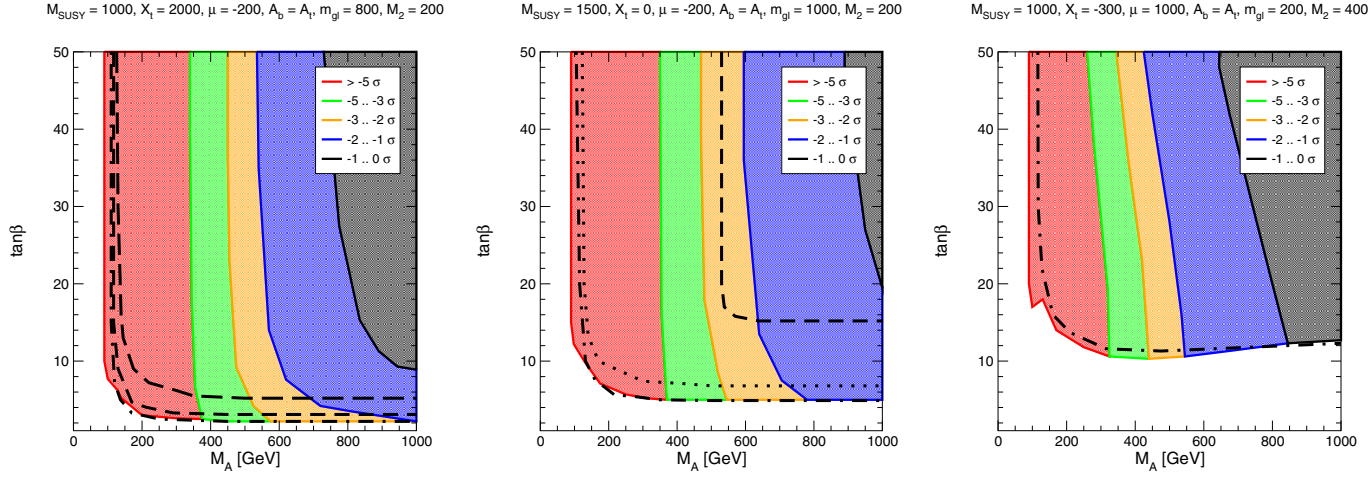

Fig. 12. The ratio R_W is shown in the $M_A, \tan\beta$ plane for the three benchmark scenarios described in the text. The observable deviation from the SM is indicated for a 5% experimental precision in R_W. The contours for the corresponding Higgs masses are also included. Dot-dashed for 113 GeV, dotted for 115 GeV, dashed for 117 GeV and long dashed for 125 GeV (Not all lines are necessarily appear in all plots)

the enhancement in R_b, these two channels are usually suppressed. There are cases in which R_W and R_γ are strongly enhanced (by a factor three or four), though these cases are not typical. Extremely strong suppressions can occur in all scenarios for $M_A \lesssim 300$ GeV, rendering these channels more difficult to observe. Deviations from the Standard Model at the 1σ level or better can be found up to $M_A \lesssim 600-1000$ GeV. Thus, these channels could also offer interesting opportunities to find deviations from the Standard Model over a wide range of MSSM parameter space.

Contrary to the unconstrained MSSM, where analyses have to be restricted to certain benchmark scenarios, the full parameter space can be explored in the CMSSM, where the soft supersymmetry-breaking scalar masses m_0 and fermion masses $m_{1/2}$ are assumed to be universal at some input unification scale. Here we restrict ourselves to $A_0 = 0$ and positive μ. An exhaustive study can be found in [47], and a similar study for the Tevatron and the LHC is given in [48].

The ratios $R_{b,W,\gamma}$ are shown in Figs. 14-16 in the $m_{1/2}$, m_0 plane for $\tan\beta = 10, 50$, $\mu > 0$ and $A_0 = 0$. Only the parameter space that gives acceptable values for a CMSSM explanation of cold dark matter, $0.1 \leq \Omega_{CDM}h^2 \leq 0.3$, is analyzed: see [**?**] for details. Correspondingly, the regions with a $\tilde{\tau}$ LSP are marked as excluded. In addition, the regions disfavored by measurements of $\mathcal{B}r(b \to s\gamma)$ [49] are indicated, as are the regions preferred by the recent $g_\mu - 2$ measurement [50].

As in the unconstrained MSSM, R_b is enhanced in the CMSSM, whereas R_W and R_γ are suppressed. Larger deviations are observed for lower values of $m_{1/2}$ and m_0, which are also preferred by the $g_\mu - 2$ measurement. For $\tan\beta = 10$, up to 3σ could be observable, whereas for

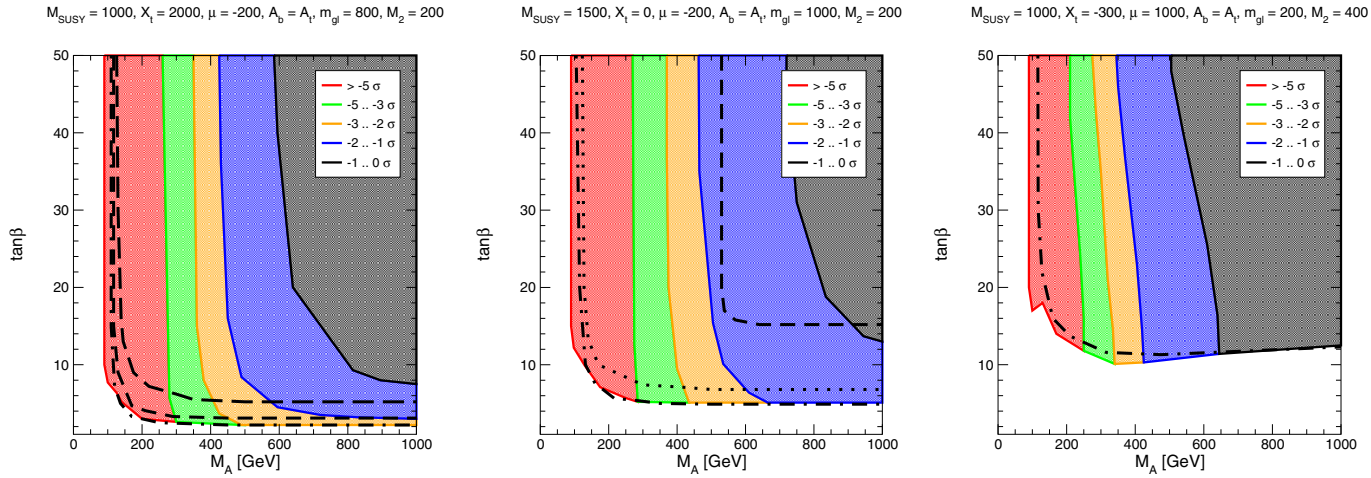

Fig. 13. The ratio R_γ is shown in the $M_A, \tan\beta$ plane for the three benchmark scenarios described in the text. The observable deviation from the SM is indicated for a 8% experimental precision in R_γ. The contours for the corresponding Higgs masses are also included. Dot-dashed for 113 GeV, dotted for 115 GeV, dashed for 117 GeV and long dashed for 125 GeV (Not all lines are necessarily appear in all plots)

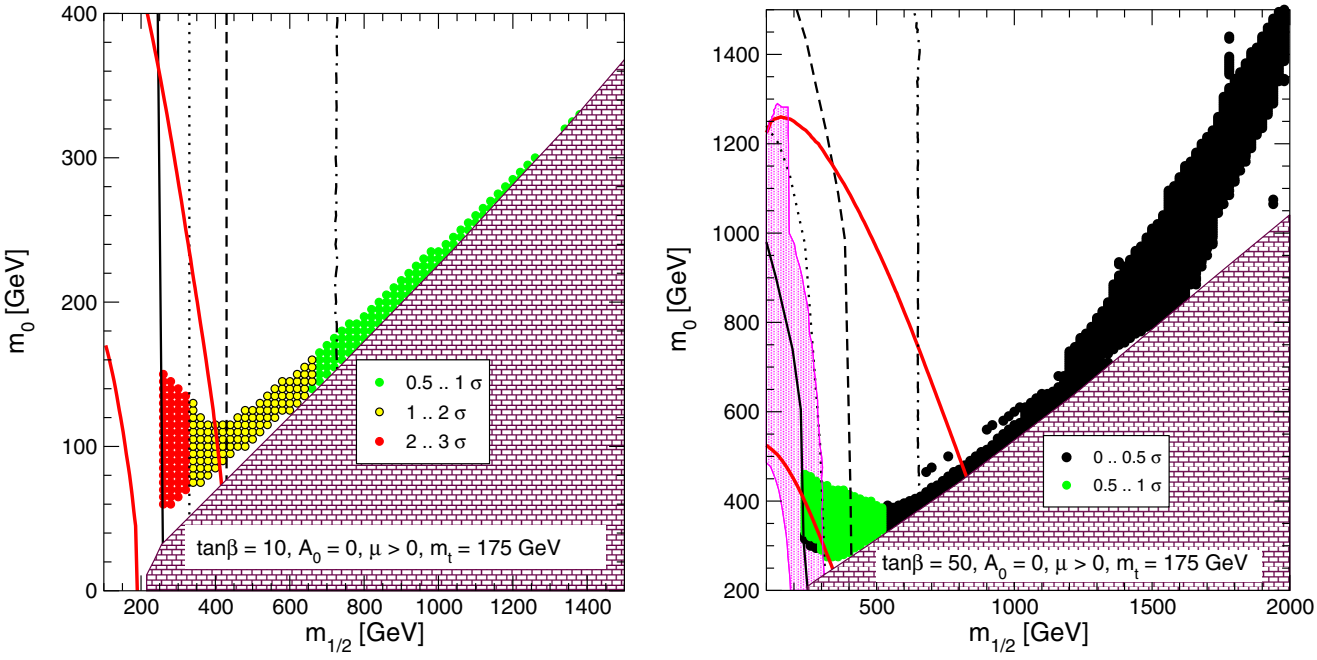

Fig. 14. The ratio R_b is shown in the $m_0, m_{1/2}$ plane for $\tan\beta = 10, 50$ and $\mu > 0$, $A_0 = 0$. The diagonal (red) solid lines are the $\pm 2\sigma$ contours for $g_\mu - 2$. The near-vertical solid, dotted and dashed (black) lines are the $m_H = 113, 115, 117$ GeV contours. The light shaded (pink) regions are excluded by $b \to s\gamma$. The (brown) bricked regions are excluded since in these regions the lightest sparticle is the charged $\tilde{\tau}_1$. The observable deviation from the Standard Model is indicated for a 2% experimental precision of R_b

$\tan\beta = 50$ the maximal deviation of the MSSM from the SM could be 2σ. Similar values would be obtainable at a linear e^+e^- collider [47]. Therefore, since it uses a different production process, a $\gamma\gamma$ collider could provide additional complementary information to the results obtainable at a linear e^+e^- collider.

Generally, it is expected that supersymmetry, if it exists, will be discovered at the LHC via the production and observation of sparticles. However one can construct also so-called Standard-Model-like scenarios where only one light Higgs boson will be within the reach of the LHC and future linear e^+e^- colliders, and its measured couplings to quarks, leptons and gauge bosons will be in agreement with their SM expectation within experimental errors.

Such scenarios can be constructed in MSSM and in more general two-Higgs-Doublet Models (2HDM), as demonstrated in [51]. In the latter study, the authors took the CP-conserving 2HDM in its model II implementation, where one doublet of fundamental scalar fields couples to the u quarks and the other to the d quarks and charged

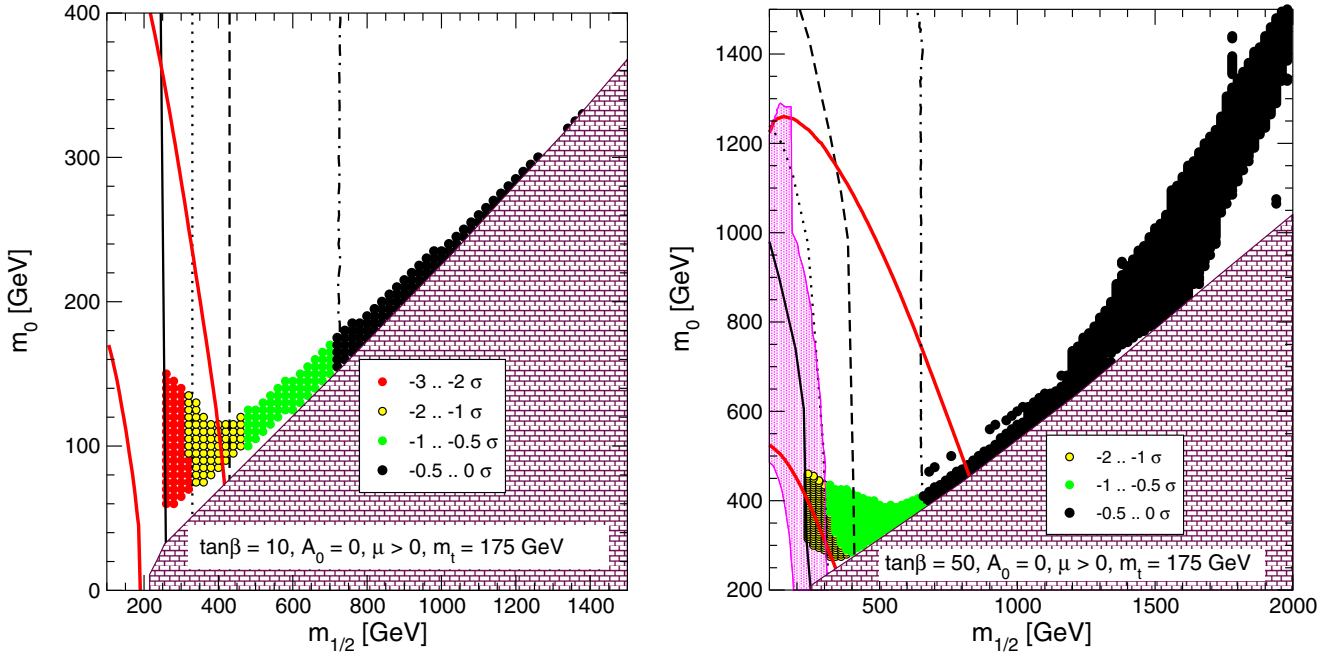

Fig. 15. The ratio R_W is shown in the $m_0, m_{1/2}$ plane for $\tan\beta = 10, 50$ and $\mu > 0$, $A_0 = 0$. The diagonal (red) solid lines are the $\pm 2\sigma$ contours for $g_\mu - 2$. The near-vertical solid, dotted and dashed (black) lines are the $m_H = 113, 115, 117$ GeV contours. The light shaded (pink) regions are excluded by $b \to s\gamma$. The (brown) bricked regions are excluded since in these regions the lightest sparticle is the charged $\tilde{\tau}_1$. The observable deviation from the Standard Model is indicated for a 5% experimental precision of R_W

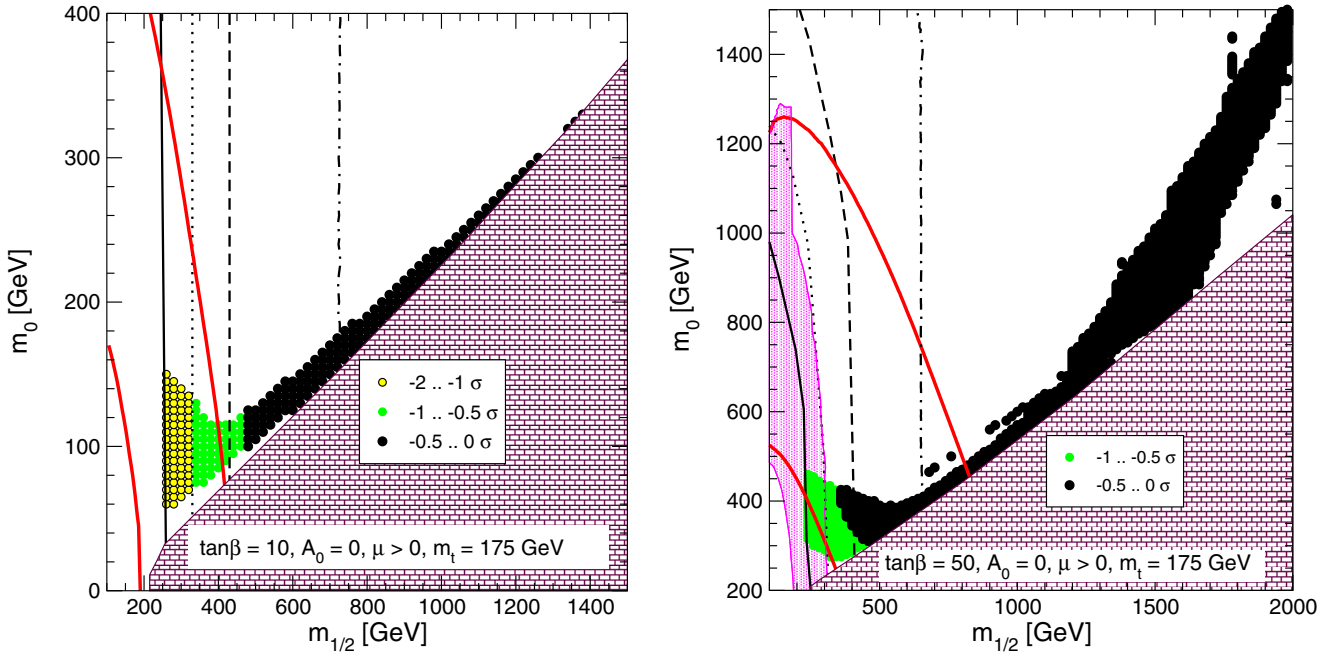

Fig. 16. The ratio R_γ is shown in the $m_0 - m_{1/2}$ plane for $\tan\beta = 10, 50$ and $\mu > 0$, $A_0 = 0$. The diagonal (red) solid lines are the $\pm 2\sigma$ contours for $g_\mu - 2$. The near-vertical solid, dotted and dashed (black) lines are the $m_H = 113, 115, 117$ GeV contours. The light shaded (pink) regions are excluded by $b \to s\gamma$. The (brown) bricked regions are excluded since in these regions the lightest sparticle is the charged $\tilde{\tau}_1$. The observable deviation from the Standard Model is indicated for a 8% experimental precision of R_γ

leptons. The experimental accuracies with which couplings are expected be measured at a 500 GeV e^+e^- linear collider are taken into account in the definition of a parameter space in the 2HDM where it would be indistinguishable from the Standard Model. Hence, the Higgs mimics all the Standard Model properties one can expect to be measured using LHC and linear collider data.

Measuring the partial width of the Higgs to photons can distinguish between such scenarios. Due to the contribution to the $H\gamma\gamma$ coupling of all charged particles, including the very heavy ones, the ratio of the Higgs boson width in the 2HDM to the one in the Standard Model can differ significantly from unity. An example is shown in Fig. 17 for a 2HDM solution which satisfies all the Standard-Model-like criteria. The possible deviation from the Standard Model for $m_H \sim 120$ GeV is considerably larger than the error in the $\gamma\gamma \to H \to \bar{b}b$ signal expected from CLICHE. This stresses the importance of accurate measurements of the two photon width of the Higgs, and the correspondingly unique role of a precision photon collider in disentangling physics beyond the Standard Model.

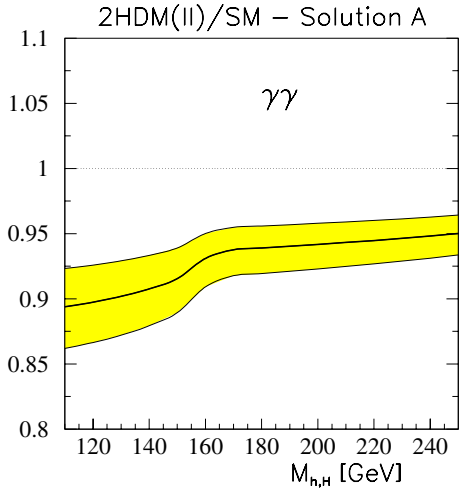

Fig. 17. Ratios of the Higgs boson $\gamma\gamma$-decay width in the 2HDM and the Standard Model as functions of $M_{h,H}$, assuming that all basic couplings are indistinguishable from those in the Standard Model [51]. $M_{h,H}$ is the mass of either of the two CP-even h or H scalar Higgs particles

3.2 QCD physics in $\gamma\gamma$ collisions

QCD aspects of $\gamma\gamma$ physics have been studied at e^+e^- colliders over the last 20 years. At LEP, $\gamma\gamma$ collisions with $E_{CM}(\gamma\gamma)$ up to 140 GeV have been studied. Up to now, the photons have been produced via bremsstrahlung [52] from the electron and positron beams, leading to soft energy spectra with only limited statistics at high $E_{CM}(\gamma\gamma)$, whereas CLICHE will produce $\gamma\gamma$ collisions in the high-energy part of the spectrum. A plethora of QCD physics topics in two-photon interactions can be addressed with a $\gamma\gamma$ collider, as recently discussed in [8]. Furthermore, good knowledge and understanding of two-photon processes will be essential for controlling physics background contributions to other processes and machine backgrounds at TeV and multi-TeV linear e^+e^- colliders.

A key issue is the total $\gamma\gamma$ cross section, which is not yet understood from first principles. Present data show a rise in $\gamma\gamma$ collisions that may be faster than that in pp, but the experimental errors are still large. At a $\gamma\gamma$ collider such as CLICHE, the photon beam energy can be tuned with a spread of less than 10%, so that measurements of $\sigma_{total}(\gamma\gamma)$ can be made at a number of 'fixed' energy values. The absolute precision with which these cross-sections can be measured ranges from 5% to 10%, according to studies made for the $\gamma\gamma$ option of TESLA [8].

Quantum fluctuations of the photon into quarks or bound states lead to the so-called hadronic structure of the photon. The absolute magnitude of the photon hadronic structure function is asymptotically determined by the strong coupling constant [53]. The classical way to study the structure of the photon is via deep inelastic electron-photon scattering, i.e., two-photon interactions with one quasi-real (virtuality $Q^2 \sim 0$) and one virtual ($Q^2 >$ few GeV^2) photon, which can be achieved by switching off one of the laser beams. Making the reasonable assumption that the scattered electron can be detected down to 25 mrad, measurements can be made in the region $5.6 \cdot 10^{-4} < x < 0.56$, where x is the fraction of the photon momentum carried by a constituent parton, and $10 < Q^2 < 8 \cdot 10^3$ GeV^2.

Although eγ scattering allows one to measure the quark distributions inside the photon, it constrains only weakly the gluon distribution, via the QCD evolution of the structure functions. Direct information on the gluon in the photon can, however, be obtained from measurements of jets [54], open charm [55] and J/ψ [56] production in $\gamma\gamma$ interactions at an $e\gamma$ and $\gamma\gamma$ collider. Values of x down to a few $\times 10^{-3}$ can be reached with charm and di-jet measurements [54,55], a region where predicted gluon distributions typically differ by a factor of two or more.

We also recall the deviation [34,35] from the NLO QCD predictions of the $b\bar{b}$ cross section in $\gamma\gamma$ collisions measured at LEP, which was mentioned earlier. It is unlikely that this matter will be settled by further analysis of the LEP data, and CLICHE could revisit the study of the $b\bar{b}$ cross section. It will allow accurate of the effective $\gamma\gamma$ center of mass energy measurements as functions of $W_{\gamma\gamma}$ and other kinematical variables to identify the origin of the putative anomaly.

A linear collider also provides circularly-polarized photon beams, which offer a unique opportunity to study the polarized parton distributions of the photon, for which no experimental data are available so far. Information on the spin structure of the photon can be obtained from inclusive polarized deep-inelastic eγ measurements and from jet and charm measurements [57,58] in polarized $\gamma\gamma$ scattering. Measurements of g_1, particularly at low x, are very important for studies of the high-energy QCD limit, where signs of the BFKL regime [59] may appear.

Other dedicated measurements have been proposed for detecting and studying the large $\ln 1/x$ logarithm resummation effects in QCD. One example is vector meson pro-

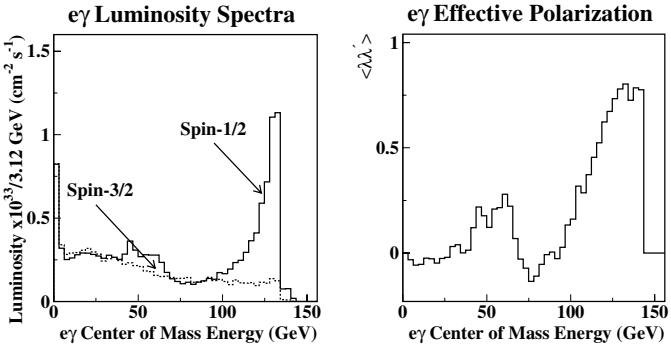

Fig. 18. Luminosity spectra and polarization for different spin states as functions of $E_{CM}(e^-\gamma)$, assuming the CLIC 1 parameters for 75 GeV electrons obtained with DIMAD [20] and CAIN [26] for $\mathcal{L}_{ee} = 4.8 \times 10^{34}\text{cm}^{-2}\text{s}^{-1}$

duction, e.g., $\gamma\gamma \to J/\psi J/\psi$ or (at large t) $\gamma\gamma \to \rho\rho$, where the hard scale in the process is given by the J/ψ mass or the momentum transfer t. The $\gamma\gamma \to J/\psi J/\psi$ cross section is around 30 pb for $E_{CM}(\gamma\gamma) \sim 120$ GeV. The J/ψ can be detected via its decay into leptons, and separated from the background via its peak in the $\ell^+\ell^-$ invariant mass. Other processes that are strongly sensitive to BFKL effects include $e\gamma$ scattering with associated jet production [60], and $e^+e^- \to e^+e^-\gamma X$ and $\gamma\gamma \to \gamma X$ [61].

3.3 $e^-\gamma$ physics

The option of $e^-\gamma$ collisions is available along with $\gamma\gamma$ and e^-e^- collisions, because the e^- conversion efficiency is, by design, less than 100%. The expected luminosity spectra for different spin states provided by the CLICHE design described previously are shown in Fig. 18. Moreover, if one wanted 50% higher $e^-\gamma$ luminosity at the peak, one could switch off one of the laser backscattering systems at cost of a factor of two in the total $e^-\gamma$ luminosity. Among the reactions of potential interest, we mention $e^-\gamma \to \nu W^-$. As seen in Fig. 19, the cross section for this process rises rapidly with $E_{CM}(e^-e^-)$ in the range accessible to CLICHE. This reaction could in principle be used to measure m_W and/or Γ_W. The result of one exploratory study is shown in Fig. 20. It shows the accuracy attainable in a measurement of Γ_W as a function of the available integrated $e^-\gamma$ luminosity. We see that a CLICHE measurement could become competitive for a luminosity of 50 fb^{-1} or more.

4 Outlook

The technology to build a machine like CLIC is under active development, but is not available today. Important progress in establishing the two-beam acceleration technique, as a novel method to obtain large gradients, has been made over the last 5 years with the CLIC Test Facilities 1 and 2. Presently, a new test facility is being prepared to demonstrate the principle of all ingredients needed to

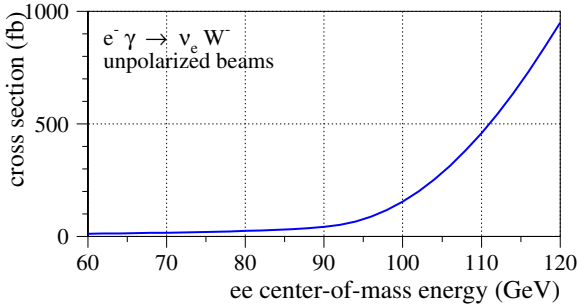

Fig. 19. The rise of the cross section for $e^-\gamma \to \nu W^-$ as a function of $E_{CM}(e^-e^-)$

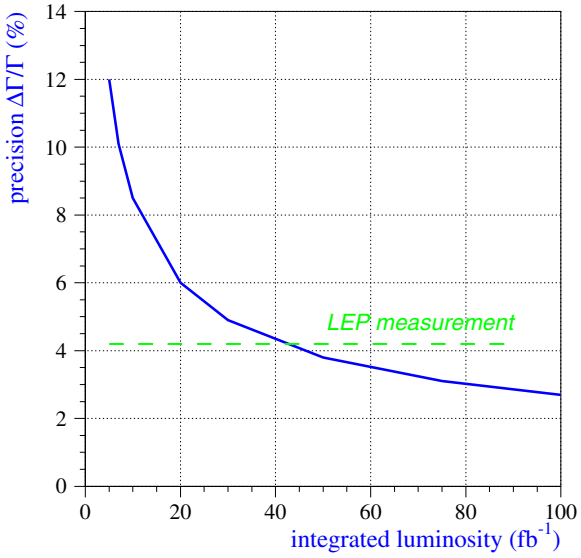

Fig. 20. The sensitivity with which Γ_W might be measured at in $e^-\gamma$ collisions, as a function of the integrated luminosity available

build up the required drive beam. The final results of this test facility are expected by the end of 2006, and, if successful, this could initiate the preparation of a Technical Design Report for a machine based on CLIC technology. As mentioned in the Introduction to this paper, the next technological step toward a multi-TeV collider could be the construction and operation of one (or, as we suggest, two) full CLIC module(s), providing acceleration by about 70 GeV. By the time one would have to define the physics objectives of such a CLIC 1 stage, it will be clear from the Tevatron and LHC if the Higgs exists and is within the mass reach of CLICHE.

In this scenario, CLICHE could be contemporary with the operation of a TeV-class e^+e^- linear collider such as TESLA, NLC or JLC. The complementary information on the Higgs boson provided by CLICHE could be very valuable and help to distinguish among models.

All the above linear collider proposals consider a $\gamma\gamma$ collider as an option that could be added to their baseline programs. The physics program of a higher-E_{CM} $\gamma\gamma$ collider has been amply documented [7,8]. Here we just recall that such a machine could provide a unique win-

dow on the heavier neutral Higgs bosons H, A expected in the MSSM and 2HDM [13,14,51], and would offer bright prospects for unraveling their CP properties. The high-energy physics program for an e^+e^- collider is by itself so rich that one can expect any photon collider option to start only several years of the start-up of the facility. The experience on photon colliders that could be gained earlier at a dedicated facility such as CLICHE could be exploited at the higher energies attainable at a TeV-scale linear collider, and eventually also at a multi-TeV collider such as CLIC [62].

Clearly the exploratory studies on machine and physics presented here need to be pursued with more detailed analyses. Ideas exist on the machine side that may lead to an increased luminosity for CLICHE. Also, it is possible that the number of lasers needed could be reduced by using recirculating laser pulses in the interaction region. If the Higgs proves to be heavier than about 125 GeV, one could also think of upgrading the input beam energy to CLIC 1.

We recall that CLICHE is just one of several possible options for doing physics with CLIC 1, many of which are more conventional and deserving serious study. However, we consider CLICHE to be a very attractive option for a project that could simultaneously validate and test all components of the CLIC technology for accelerating high-energy beams and can give important scientific output, covering a unique facet of the study of the Higgs boson, whose study will be central to physics at the high-energy physics frontier over the next decade or two.

Acknowledgements. This work was performed in part under the auspices of the U.S. Department of Energy by the University of California, Lawrence Livermore National Laboratory under Contract No.W-7405-Eng.48, and the Illinois Consortium for Accelerator Research, ICAR.

References

1. The CLIC Study Team, G. Guignard (ed.), A 3 TeV Linear Collider Based on CLIC Technology, CERN 2000-008 (2000)
2. The CTF Team, H. H. Braun (ed.), Experimental Results and Technical Results and Development at CTFII, CERN-PS-2000-030-AE (2000)
3. R.D. Heuer, D. Miller, F.Richard, P.M. Zerwas (eds.) et al., TESLA TDR, Part III: Physics at an e^+e^- Linear Collider, Report DESY-01-011C, http://arXiv.org/abs/hep-ph/0106315
4. T. Abe, et al., Linear Collider Physics Resource Book for Snowmass 2001 - Part 3: Studies of Exotic and Standard Model Physics,
BNL-52627, CLNS 01/1729, FERMILAB-Pub-01/058-E, LBNL-47813, SLAC-R-570, UCRL-ID-143810-DR, LC-REV-2001-074-US, http://arXiv.org/abs/hep-ex/0106057
5. R. Hawkings, K. Mönig, Eur. Phys. J. direct C **8**, 1 (1999); J. Erler, S. Heinemeyer, W. Hollik, G. Weiglein, P.M. Zerwas, Phys. Lett. B **486**, 125 (2000); J. Erler, S. Heinemeyer, http://arXiv.org/abs/hep-ph/0102083
6. V. Telnov, Nucl. Instrum. Meth. A **355**, 3 (1995); I. F. Ginzburg, G. L. Kotkin, V. G. Serbo, V. I. Telnov, Nucl. Instr. Meth. **205**, 47 (1983); I. F. Ginzburg, G. L. Kotkin, S. L. Panfil, V. G. Serbo, V. I. Telnov, Nucl. Instr. Meth. A **219**, 5 (1984)
7. NLC Collaboration, 2001 Report on the Next Linear Collider: A Report Submitted to Snowmass 2001, SLAC-R-571, FERMILAB-CONF-01-075-E, LBNL-PUB-47935, UCRL-ID-144077, June 2001
8. B. Badelek, et al., TESLA TDR, Part IV: The Photon Collider at TESLA, http://arXiv.org/abs/hep-ex/0108012
9. The LEP Collaborations, the LEP Electroweak Working Group and the SLD Heavy Flavour and Electroweak Groups, CERN/EP-2001/021
10. ALEPH, DELPHI, L3 and OPAL Collaborations, LEP working group for Higgs boson searches, preprint CERN-EP/2001-055, http://arXiv.org/abs/hep-ex/0107029
11. Y. Okada, M. Yamaguchi, T. Yanagida, Prog. Theor. Phys. **85**, 1 (1991); J. R. Ellis, G. Ridolfi, F. Zwirner, Phys. Lett. B **257**, 83 (1991); H. E. Haber, R. Hempfling, Phys. Rev. Lett. **66**, 1815 (1991); M. Carena, J. R. Espinosa, M. Quiros, C. E. Wagner, Phys. Lett. B **355**, 209 (1995); M. Carena, M. Quiros, C. E. Wagner, Nucl. Phys. B **461**, 407 (1996); H.E. Haber, R. Hempfling, A.H. Hoang, Zeit. für Phys. C **75**, 539 (1997); S. Heinemeyer, W. Hollik, G. Weiglein, Eur. Phys. Jour. C **9**, 343 (1999); J. R. Espinosa, R. Zhang, Nucl. Phys. B **586**, 3 (2000)
12. D. Schulte, F. Zimmermann, Accelerator Aspects of a Potential CLIC 1 Collider, CLIC-Note 496 (2001)
13. M.M. Mühlleitner, M. Krämer, M. Spira, P.M. Zerwas, Phys. Lett. B **508** (2001)
14. D. Asner, et al., UCRL-ID-143967 (2001), to be submitted to Phys. Rev. D , http://arXiv.org/abs/hep-ph/0110320
15. R. Corsini, for the CTF3 Study Team, An Overview of the New CLIC Test Facility (CTF3), CERN-PS-2001-030-AE; CLIC-Note-485; presented at the IEEE Particle Accelerator Conference, Chicago, IL, USA, 18-22 June 2001
16. Stanford Linear Accelerator Center, SLAC Linear Collider Conceptual Design Report, SLAC-Report-229 (1980)
17. L. Evans, R. Schmidt, CLIC Damping Ring in the SPS Tunnel, SPS/DI/Note/88-1 (1988)
18. J.M. Jowett, T. Risselada, F. Zimmermann, H. Owen, Damping rings for CLIC, CERN-SL-2001-038-AP; CLIC-NOTE-494; CERN-CLIC-NOTE-494; presented at the IEEE Particle Accelerator Conference (PAC 2001), Chicago, IL, USA, 18-22 June 2001
19. P. Raimondi, A. Seryi, New developments in linear colliders final focus systems, Proc. of the 20th Intl. Linac Conference LINAC 2000 ed. Alexander W. Chao, eConfC **000821**, MO301 (2000), http://arXiv.org/abs/physics/0008072
20. R. Servranckx, K. L. Brown, L. Schachinger, D. Douglas, SLAC-0285; http://www-project.slac.stanford.edu/lc/local/AccelPhysics/Codes/Dimad/
21. D. Schulte, PLACET: a Program to Simulate Drive Beams, CERN-PS-2000-028-AE; CLIC-Note-437 (2000); presented at the 7th European Particle Accelerator Conference, Vienna, Austria, 26-30 June 2000
22. D. Schulte, TESLA-97-08 (1996)
23. Y. Yasui et al., http://arXiv.org/abs/hep-ph/9212312
24. I. Watanabe et al., Gamma Gamma Collider as an Option of JLC, KEK-REPORT-97-17, AJC-HEP-31, HUPD-9807, ITP-SU-98-01, DPSU-98-4, March 1998

25. A. Djouadi, J. Kalinowski, M. Spira, Comput. Phys. Commun. **108**, 56 (1998)
26. P. Chen, G. Horton-Smith, T. Ohgaki, A. W. Weidemann, K. Yokoya, Nucl. Instrum. Meth. A **355**, 107 (1995); See http://www-acc-theory.kek.jp/members/cain/cain21b.manual/main.html
27. T. Sjostrand, http://arXiv.org/abs/hep-ph/9508391; T. Sjostrand, P. Eden, C. Friberg, L. Lonnblad, G. Miu, S. Mrenna, E. Norrbin, http://arXiv.org/abs/hep-ph/0010017; See the PYTHIA and JETSET webpages, http://www.thep.lu.se/torbjorn/Pythia.html
28. M. Peskin et al., details can be obtained from http://www-sldnt.slac.stanford.edu/nld/new/Docs/Generators/PANDORA.htm and http://www.slac.stanford.edu/mpeskin/LC/pandora.html
29. FASTMC is supported by the NLC Group at SLAC. Details can be obtained from http://www-sldnt.slac.stanford.edu/nld/documentation/fastmc/
30. T. Ohgaki, Int. J. Mod. Phys. A **15**, 2605 (2000)
31. M. Schmitt, D. Stenz, M. Velasco, to be submitted to Eur. Phys. Jour., NUHEP-EXP/02-002, http://lotus.phys.nwu.edu/schmittm/nuhep-exp
32. T. Ohgaki, et al., Phys. Rev. D **56**, 1723 (1997)
33. G. Jikia, S.Soldner-Rembold, Light Higgs Production at a Photon Collider, submitted to International Workshop on High Energy Photon Colliders, June 14 - 17, 2000, DESY Hamburg, Germany, http://arXiv.org/abs/hep-ex/0101056
34. L3 Collaboration, P. Achard et al., CERN-EP/2000-144 (2000)
35. OPAL Collaboration, OPAL Physics Note PN455 (2000)
36. M. Dittmar, H. Dreiner, Phys. Rev. D **55**, 167 (1997)
37. M.Battaglia, K.Desch, Physics and Experiments with Future Linear e^+e^- Colliders, A. Para, H.E. Fisk (editors) AIP Conf. Proc. **578**, 163 (2001)
38. G.J. Gounaris, G.P. Tsirigoti, Phys. Rev. D **56**, 3030 (1997); Erratum - ibid. D **58**, 059901 (1998)
39. K. Hagiwara, Nucl. Instrum. Meth. A **472**, 12 (2001)
40. M. Velasco et al., Photon-Photon and Electron-Photon Colliders with Energies Below a TeV, Summary of the Snowmass 2001 E2-SO2 Working Group, contributed paper E3-005, http://arXiv.org/abs/hep-ex/0111055
41. S. Dawson, talk at the Second International Workshop on High-Energy Photon Colliders, Fermilab, Batavia, Illinois, March 14-17, 2001, available from http://diablo.phys.nwu.edu/ggws/
42. S. Heinemeyer, W. Hollik, G. Weiglein, Comput. Phys. Commun. **124**, 76 (2000); http://arXiv.org/abs/hep-ph/0002213; the FeynHiggs code is available from http://www.feynhiggs.de
43. S. Heinemeyer, W. Hollik, G. Weiglein, Phys. Rev. D **58**, 091701 (1998); Phys. Lett. B **440**, 296 (1998); Eur. Phys. Jour. C **16**, 139 (2000)
44. M. Carena, S. Heinemeyer, C. Wagner, G. Weiglein, http://arXiv.org/abs/hep-ph/9912223
45. R. Barate et al. [ALEPH Collaboration],Phys. Lett. B **499**, 53 (2001)
46. M. Carena, H. E. Haber, H. E. Logan, S. Mrenna, Phys. Rev. D **65**, 055005 (2002)
47. J. R. Ellis, S. Heinemeyer, K. A. Olive, G. Weiglein, in preparation
48. J. R. Ellis, S. Heinemeyer, K. A. Olive, G. Weiglein, Phys. Lett. B **515**, 348 (2001); J. R. Ellis, J.S. Hagelin, D.V. Nanopoulos, K.A. Olive, M. Srednicki, Nucl. Phys. B **238**, 453 (1984); see also H. Goldberg, Phys. Rev. Lett. **50**, 1419 (1983); J. R. Ellis, T. Falk, G. Ganis, K. A. Olive, M. Srednicki, Phys. Lett. B **510**, 236 (2001)
49. CLEO Collaboration, S. Chen et al., CLEO CONF 01-16, submitted to Phys. Rev. D; K. Abe et al., Belle Collaboration, http://arXiv.org/abs/hep-ex/0103042; G. Degrassi, P. Gambino, G. F. Giudice, JHEP **0012**, 009 (2000); see also M. Carena, D. Garcia, U. Nierste, C. E. Wagner, http://arXiv.org/abs/hep-ph/0010003
50. H. N. Brown et al., Muon $g_\mu - 2$ Collaboration, Phys. Rev. Lett. **86**, 2227 (2001); A. Czarnecki, W. J. Marciano, Phys. Rev. D **64**, 013014 (2001), http://arXiv.org/abs/hep-ph/0102122
51. I.F. Ginzburg, M. Krawczyk, P. Osland, Physics, Experiments with Future Linear e^+e^- Colliders, A. Para, H.E. Fisk (editors) AIP Conf. Proc. **578**, 304 (2001)
52. C. F. Weizsäcker, Z. Phys. **88**, 612 (1934); E. J. Williams, Phys. Rev. **45**, 729 (1934)
53. E. Witten, Nucl. Phys. B **120**, 189 (1977)
54. T. Wengler, A. De Roeck, Proc. of the Workshop on Photon Colliders, DESY, Hamburg, June 2000, http://arXiv.org/abs/hep-ph/0010293
55. P. Jankowski, M. Krawczyk, A. De Roeck, LC-TH-2000-034, http://arXiv.org/abs/hep-ph/0002169
56. R. M. Godbole, D. Indumathi, M. Krämer, LC-TH-2001-019 (2001)
57. M. Stratmann, Nucl. Phys. Proc. Suppl. **82**, 400 (2000), http://arXiv.org/abs/hep-ph/9907467
58. J. Kwiecinski, B. Ziaja, Phys. Rev. D **63**, 054022 (2001)
59. E.A. Kuraev, L.N. Lipatov, V.S. Fadin, Sov. Phys. JETP **45**, 199 (1972); Y.Y. Balitsky, L.N. Lipatov, Sov. J. Nucl. Phys. **28**, 822 (1978)
60. G. Contreras, A. De Roeck, LC-TH-2001-031 (2001)
61. N. Evanson, J. Forshaw, LC-TH-2000-010, http://arXiv.org/abs/hep-ph/9912487
62. H. Burkhardt, Nucl. Instrum. Meth. A **472**, 67 (2001)